CZECH TECHNICAL UNIVERSITY IN PRAGUE

Faculty of Nuclear Sciences and Physical Engineering

Department of Physics

Bachelor's thesis

Measurement of distributions sensitive to underlying event at the LHC at 13 TeV

Matouš Vozák

Supervisor: Mgr. Oldřich Kepka, Ph.D.

Praha, 2015

ČESKÉ VYSOKÉ UČENÍ TECHNICKÉ
V PRAZE
Fakulta Jaderná a Fyzikálně Inženýrská
Katedra Fyziky

Bakalářská práce

Měření spekter citlivých na underlying event na LHC při těžišťové energii 13 TeV

Matouš Vozák

Supervisor: Mgr. Oldřich Kepka, Ph.D.

Praha, 2015

NASCANOVAT PODEPSANE ZADANI A
ULOZIT DO DVOU EPS SOUBORU
ZADANI1.EPS a ZADANI2.EPS

NASCANOVAT PODEPSANE ZADANI A
ULOZIT DO DVOU EPS SOUBORU
ZADANI1.EPS a ZADANI2.EPS

Prohlášení:

Prohlašuji, že jsem svou bakalářskou práci vypracoval samostatně a použil jsem pouze podklady (literaturu, projekty, SW atd ...) uvedené v přiloženém seznamu.

Nemám závažný důvod proti použití tohoto školního díla ve smyslu § 60 Zákona č. 121/2000 Sb., o právu autorském, o právech souvisejících s právem autorským a o změně některých zákonů (autorský zákon).

V Praze dne

Title:
Measurement of distributions sensitive to underlying event at the LHC at 13 TeV

Author: Matouš Vozák

Specialization: Experimental nuclear and particle physics

Sort of project: Bachelor's thesis

Supervisor: Mgr. Oldřich Kepka, Ph.D

Abstract: In proton-proton collisions there are phenomena such as interaction between more than one pair of partons or parton showers which represent additional activity to any hard process and are collectively termed as underlying event. Brief introduction to the theory of proton-proton collision along with the first measurement of this additional activity at the LHC at 13 TeV are presented. Distributions of transverse momentum and number of particles are studied in three regions with a different sensitivity to the underlying event. The underlying event activity is roughly 20% higher at 13 TeV than at 7 TeV. This early measurement also presents comparison of selection of MC models with data and provides validation of UE modeling for ATLAS simulations.

Key words: Underlying event, Monte Carlo, LHC at 13 TeV, multiparton interaction, initial and final state radiation, ATLAS, transverse momentum, pseudorapidity.

Název práce:
Měření spekter citlivých na underlying event na LHC při těžišťové energii 13 TeV

Autor: Matouš Vozák

Specializace: Experimentální Jaderná a Částicová Fyzika

Projekt: Bakalářská práce

Školitel: Mgr. Oldřich Kepka, Ph.D

Abstrakt: V proton-protonových srážkách existují jevy jako například interakce mezi více než jedním párem partonů nebo partonové spršky, které představují dodatečnou aktivitu k těžkým procesům a které jsou souhrně nazývány underlying event. Náplní práce je krátký úvod do teorie proton-protonových interakcí společně s měřením této dodatečné aktivity na LHC při 13 TeV. Distribuce příčných hybností a počtu částic jsou studovány ve třech oblastech s různou aktivitou underlying eventu. Tato aktivita je zhruba o 20% vyšší na 13 TeV než na 7 TeV. V tomto brzkém měření je poskytnuto porovnání vybraných Monte Carlo modelů s daty a také vyhodnocení underlying event modelů pro simulaci detektoru ATLAS.

Klíčová slova: Underlying event, Monte Carlo, LHC na 13 TeV, multipartonové interakce, počáteční a finální radiace, ATLAS, příčná hybnost, pseudorapidita.

Acknowledgement

First, I would like to thank Mgr. Oldřich Kepka, Ph.D. for his guidance, patience, friendly approach, great opportunities and shared wisdom. My thanks also go to my family and friends who supported me the whole time and gave me the strength.

Contents

List of Figures

Chapter 1

Introduction

The world is a place rich on particles. Some of them are already known some of them are about to be discovered. Particles differ in many aspects but one of the most important thing is their mass (some don't have a mass e.g photon). As is well known today from Einstein's special theory of relativity mass is related to energy, therefore to acquire a particle with a certain amount of mass a necessary amount of energy have to be supplied to create the particle of interests. For that reason accelerators exist. There are several types of accelerators. To obtain high energy particles people use colliders, in which particles are accelerated in both directions and then they are directed to collide with each other. One of the most well known collider is the LHC (Large Hadron Collider) which is situated on the border between Switzerland and France. However, the collision environment can be busier and have more participants. For example particles can be created through radiation of charged colliding objects or in case of composite colliding particles , such as protons, more than one of its constituent (parton) can attend the collision (Multi-parton interaction) and of course there can still be remnants of collided objects. All of these processes bring additional activity to the event and are generally termed as the "Underlying event" (UE).

This additional activity can represent contamination to the measurements. One example can be measuring of groups of collimated particles (jets). The UE is negligible for jets with transverse momentum p_T (Chapter 4) around 200 GeV and higher but as p_T goes to the lower values (20 GeV) the UE affect the measurement and has to be accounted for. Therefore, it is necessary to study the UE to know the ambient activity.

In collision there can be processes where a lot of transverse momentum is transferred between the initial and final states. These processes are called "hard" and can be calculated from perturbative theory. On the other hand there could be processes with a small transverse momentum change. These are referred as "soft" and they very often accompany the hard ones. The drawback of soft processes is that they cannot be calculated from perturbative or any other theory hence approximation method to successfully describe them is required. One way to do so is through Monte Carlo (MC) generators.

These generators are tools used to get results which are later on compared with the real data. There are several models implemented in MC generators representing soft interaction. Generators also contain several "free" parameters. It is necessary to find the right values of these parameters (this method is called "tuning") so that the MC match well the real data. Parameters might be correlated and hence have to be changed simultaneously. Examples of MC generators are Pythia, Herwig, Epos, ...

The contribution of the UE to the process can be described by observables which represent collective effects of the event. Example of such observable is $< d^2N_{ch}/d\eta d\phi >$ (mean number of charged particles per unit pseudorapidity η and azimuthal angle ϕ). Common approach is to study these observables in three different regions (Fig. 1.1) which are defined with respect to the particle with the highest transverse momentum.

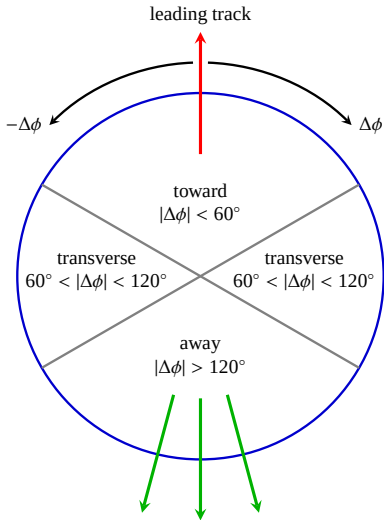

Fig. 1.1: Region selection in xy plane with respect to the leading track (particle with the highest transverse momentum)[4].

The UE observables has been already measured in $p\bar{p}$ collisions at $\sqrt{s} = 1.8$TeV and 1.96 TeV in dijet and Drell-Yan events at CDF in Run I [1] and Run II [2], in pp collisions at $\sqrt{s} = 900$ GeV in a detector-specific study by CMS [3] and also in pp collisions at $\sqrt{s} = 900$ GeV and $\sqrt{s} = 7$ TeV at the LHC performed by the detector ATLAS [4]. This thesis focuses also in pp collisions at the LHC measured by the ATLAS but with the central mass energy 13 TeV.

The structure of this thesis goes as follows. Firstly, several important points from the Standard model are introduced in Chapter 2, followed by description of different kinds of collision in Chapter 3. The purpose of Chapter 4 is to explain or remind a few variables used in collider physics. How the inner structure of the proton was discovered and explained contains Chapter 5. Short introduction of the main steps in the theory of MC generators provides Chapter 6 and the brief description about the most important parts of the ATLAS detector for this thesis is in Chapter 7. The experimental part of this thesis with results can be found in Chapter 8 and finally the summary is in Chapter 9.

Chapter 2

Standard model (SM)

The more man explores nature and mysteries behind it the more he realizes how vast and deep it can be. From Greeks who started putting together the buildings blocks of physics based mainly on philosophical view (Leukipos-word is composed of atoms), humanity managed to get to the point of being able to predict something (particle) which has strong foundation in mathematics and prove its existence by various experiments (Discovery of Higgs Boson). Undoubtedly, since Leukiposs there has been a huge progress in physics and science in generall but even more development is surely to come. The Standard Model of elementary particle physics (SM) is not a complete summary of physics knowledge but covers most of todays experimental evidence on how "this" world works. As it is not only theoretical approach to the physics, SM contains several input parameters which need to be found experimentally.

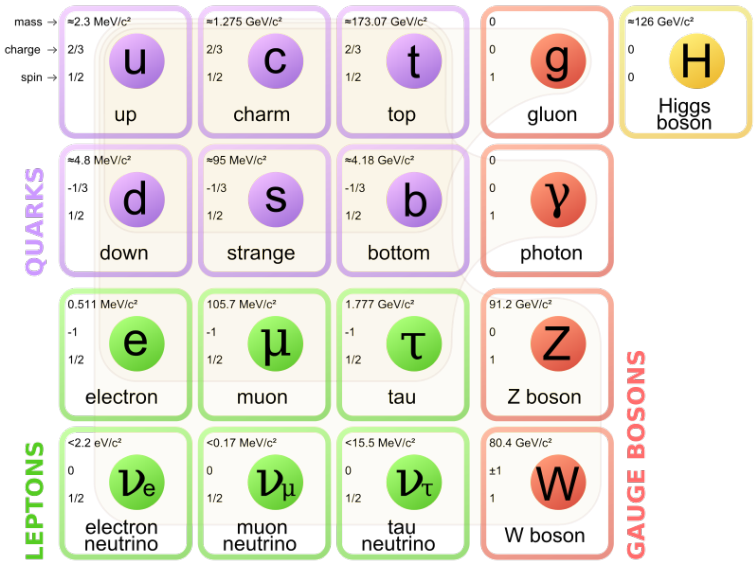

Fig. 2.1: The table of elementary particles [5].

Elementary particle is a term for a particle with no evidence of inner substructure. In Fig. 2.1 there are so far all known and experimentaly proved elementary particles. Each particle is either a boson

or a fermion depending on its spin, the quantum number which in simplified way can be viewed as an intrinsic angular momentum. If the spin of particle is half-integer than the particle is a fermion, on the other hand if the spin is integer the particle is boson (masses of fermions and bosons are for example the already mentioned parameters of SM). There are five bosons in Fig. 2.1 including the recent experimentally proved Higgs particle. Except the Higgs there are 4 mediators of fundamental interactions called gauge bosons, which will be discussed later on. As can be seen in the mentioned figure there are also particles called quarks. Everything composed of quarks is called a hadron. Composed particles can consist of three quarks and are called baryons (for example proton p) or of two quarks which are termed mesons (π meson). There are three generations of quarks grouped together according to their masses. The quarks carry not only an electric charge but also a colour charge (discussed later) and because of that they are subject to the strong interaction. The particles on which this interaction does not act are called Leptons. There are also three generation of leptons and more likely there will not be another with the mass below mass of Z boson m_Z (If the total number of lepton generation is three it fits well Z resonance). Leptons as electron, muon and tauon are electricaly charged but there are additional neutral particles within each generation termed neutrinos.

There are four known elementary interactions. Weak, electromagnetic, strong and gravitational. The first three are covered in SM (Tab. 2.1), gravity is not. The idea is that all four of them come from one universal interaction therefore can be unified at some level. The problem is that there hasn't been success to integrate gravity with the rest. There are of course attempts such as string theory which is actually able to do so but for that it needs 11 dimensions and that is a bit hard to understand. Therefore the SM works only with weak, electromagnetic and strong interaction. Each one of them is mediated by the exchange of gauge bosons.

Interaction	gauge boson	Mass (GeV/c^2)	J^P	Range (m)
weak	$W^{\pm}$, Z^0	$\approx$ 80, 91	1	10^{-18}
electromagnetic	photon	0	1^-	∞
strong	gluon	0	1^-	$\leq 10^{-15}$

Tab. 2.1: Three fundamental interaction with their range and some aspect of their corresponding gauge bosons - mass, total spin J and parity P.

The weak interaction is mediated by $W^{\pm}, Z$ bosons which have a large mass therefore the range of weak interaction is the smallest of all interactions in the SM. The weak interaction is responsible for β decay, a type of radiation discovered by E. Rutherford along with α and γ. There are two types of β decay $\rightarrow \beta^+$, β^-. In β^+protons through weak interaction decay into neutron and pozitron (cannot happen with free proton, only in nucleus) and in β^- neutrons into proton and electron. Except these two charged particles, β^+/β^- gives birth also to the third most numerous particle of all particle to antineutrino/neutrino. The weak interaction is the second weakest interaction right after gravity.
Massles particles ,photons, are gauge bosons for electromagnetic interaction. Contrary to the weak interaction, the effect of electromagnetism spreads to infinity. The force in question occurs between particles carrying electric charge either positive $+e$ (for example proton) or negative $-e$ (electron). Due to the electromagnetic force electrons interact with the nuclei and are bound to the atom. In addition these electrons interact repulsively with electrons from other atoms. Because of this interaction between electrons it is not possible to go through a concrete wall so easily.

Strong interaction acts also between charged particles but in this case the charge is represented as something called colour. There cannot be two fermions in an identical (quantum) state according to Pauli exclusion principle. However some particles as Ω baryon (Ω(sss)) contain 3 quarks with the same

flavour. To preserve Pauli principle it was necessary to introduce new degree of freedom which is the already mentioned colour. There are 3 colour charges red, green, blue and in addition, their anti-colour charges anti-red, anti-green and anti-blue. The colour charge is an analogue to electric charge. White colour, which is obtainable by adding together red, green and blue colour, is representing neutral objects such as baryons and mesons. Therefore it is possible for a particle to be composed of three quarks with the same flavour, but each one of them must have different colour. Except quarks, gluons are also carriers of charge. Each gluon carry one charge and one anti-charge and that is an enormous difference between electromagnetism and strong interaction. Photons do not transfer electric charge but because gluons do so, it is possible for gluon to interact with each other (Fig. 2.2). This leads to asymptotic freedom which describes behaviour of strong interaction between two quarks. This behaviour with respect to the distance between quarks can be also seen in Fig. 2.2. As can be interpreted from mentioned figures the more are quarks away from each other the more they feel the force pulling them back. It is not possible to observe free quarks and gluons. Instead, they are bound to hadrons because as soon as they are separeted new quarks will immediately pair up with them creating a new hadron. The strong interaction is the one that holds nucleus together. As the name implies it is the strongest among fundamental forces. Without it protons would not be able to stay together due to the coulomb force pulling them away.

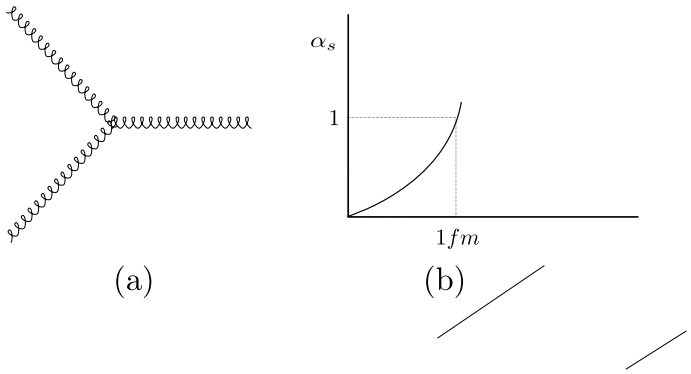

Fig. 2.2: a) Self-gluon interaction, (b) dependence of structure constant α_s on the distance between strongly interacting objects.

The first unification between interactions was done by J.C. Maxwell who through his equation put together electricity with magnetism in 1865. The important steps in physics were discovery of special theory of relativity (1905) and quantum mechanics (first half of the 20th century). At the end of 60-ties Weinberg with Salam realized that originally there used to be a force which was named electro-weak with four gauge bosons all of them massles but due to the symmetry breakdown it was separated into weak and electromagnetic force. In the second half of the 20th century quantum version of electromagnetism QED (quantum electrodynamics) were introduced along with the description of behaviour of strong interaction QCD (quantum chromodynamics). Some of the particles interact both strongly and weakly therefore there is also relation between QED and QCD putting only gravity aside. The standard model contains not only topics discussed above but many more such as violation of symmetries, generation mixing, etc. The SM also does not answer all question: Why only three families of leptons exist? Why are there only four interactions? Can gravity be really included to the SM? It also assume that neutrinos are massless but effect of neutrinos oscillation has been observed which is only possible if neutrinos have mass. Nevertheless the theory included in the SM agrees with many experiments hence it can be said that the SM works.

Chapter 3

Introduction to particle collisions

There are several devices which are able to accelerate particles such as linear accelerators, cyclotrons, betatrons but for the creation of high energy particles it is more convenient to use colliders. The reason lies in the conservation of momentum. For example, in the case of linear accelerator the accelerated particles are shot at the target (Fig. 3.1). The particles from the target are kicked out and to conserve the momentum before and after collision lots of energy is transfered to the kinetic energy of the whole produced system.

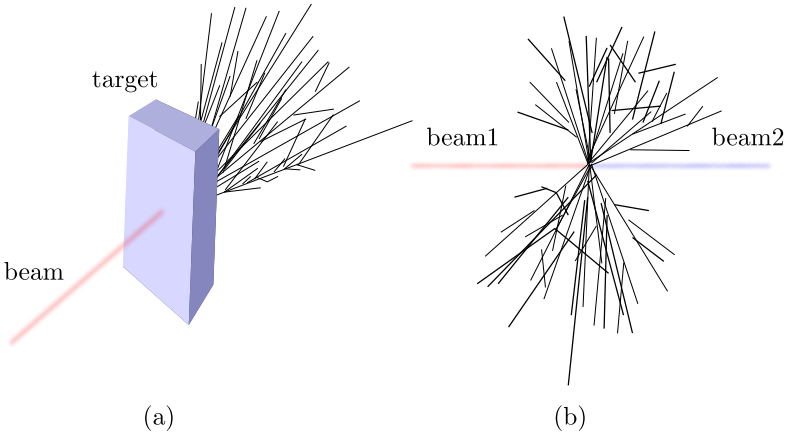

Fig. 3.1: Cartoon of collisions performed by (a) linear accelerator and (b) collider.

That is not the case with colliders. Colliding particles have approximatly the same energy and opposite momentum therefore there are less constraint for kinetic energy to conserve the momentum and more energy from the collision can be used to create new particles. With that thougt in mind, people try to collide different objects as electrons with positrons (experiments PETRA, HERA, ...), heavy nucleus with protons, protons with protons (the LHC) and others. As this thesis concerns the proton proton collisions only the character of collisions in question will be discussed.
It is experimentally proved fact that protons are composite objects (Chapter 5) and as such the character of their collision tends to be more vivid than electron collisions. In classical mechanic there are two types of collision between objects. The first one is called elastic collision. It is said that the particle collided elastically when both "mechanic" (sum of potential and kinetic) energy and momentum conservations apply. In particle physics (on much lower scales) it is similar as in classical mechanics. There are also elastic and inelastic collisions but the word collision is substituted by "scattering" due to the quantum mechanical effect in particular wave-particle duality. In the elastic scattering two particles interact (for example electromagnetically) and only change their trajectories. On the other

hand, protons are dissociated to its constituent in inelastic scattering events. There are three types of inelastic events. Single diffraction, double diffraction and non-diffraction (Fig. 3.2). In a single

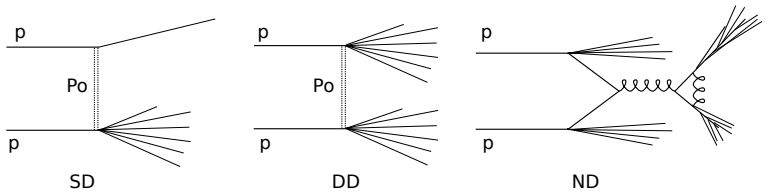

Fig. 3.2: SD-single diffraction, DD-double diffraction and ND-non diffraction of two incoming protons p (with exchange of Pomeron Po in SD, DD).

diffraction only one proton is disociated without colour exchange between the protons (exchange of hypothetical particle Pomeron) and double diffraction is accompanied with disociation of both protons. Unlike the previous diffractive cases there is a colour change in non diffractive collision.

Chapter 4

Variables

The purpose of this chapter is to introduce variables, constants and units which readers will eventualy meet in the theory section or in the chapter where measurements are discussed.

4.1 Central mass energy (CMS)

Protons which are accelerated at the LHC moves relativisticaly (velocity of the proton at central mass energy 7 TeV is around 0.999999991 speed of light!) meaning that we cannot use a classical mechanics to do the physics but the special theory of relativity (STR). For the understanding and definition of the variables it is necesary to have some knowledge of the STR [6].
Assume two particles with energies E_1, E_2 and (three) momentums $\vec{p_1}$, $\vec{p_2}$ then the four vector of the system P^μ (in natural units) will be

$$P^\mu = \begin{pmatrix} E_1 + E_2 \\ \vec{p}_1 + \vec{p}_2 \end{pmatrix}. \tag{4.1}$$

From four vector the invariant $P^\mu P_\mu$ can be computed.

$$P^\mu P_\mu = (E_1 + E_2)^2 - (\vec{p}_1 + \vec{p}_2)^2 \tag{4.2}$$

If the coordinate system is set to the center of mass $\vec{p}_1 = -\vec{p}_2$. With assumption that both particles have approximately the same energy $E_1 = E_2 = E_{CM}/2$, (4.2) can be modified.

$$P^\mu P_\mu = (E_{CM})^2 \tag{4.3}$$

E_{CM} is reffered as the central mass energy and was already mentioned in the introduction. In many publications the central mass energy is more often marked as $\sqrt{s}$ than E_{CM} ($s = E_{CM}^2$) and this thesis will also hold the notation with $\sqrt{s}$.

4.2 Transverse momentum

Classical cordinate system for particle collision (used for example for ATLAS detector) is with z-axis along the beam pipe (counterclokwise), x-axis pointing at the center of the LHC ring and y-axis oriented upwards. The transverse momentum p_T is then defined as following

$$p_T = \sqrt{p_x^2 + p_y^2}. \tag{4.4}$$

Measuring p_T has some advantages. Firstly, transverse momentum is Lorentz invariant along the propagation axes z (another aspect of STR). The second reason lies again in conservation. The particles

are collimated with such precision that the transverse momentum before the collision is approximately equal to zero and that is what is expected also after the collision due to momentum conservation. It is not technically possible to build a sphere detector for colliders because the particles have to enter the detector from somewhere hence detectors are built around the beam pipe (pipe in which particles travel). Therefore there are gaps on each side where there are no detectors. In elastic collisions particles only slightly change their momentum and some of them are not detectable because after the interaction they will go through the detector gap. But these particles will have only minimal transverse momentum therefore their contribution to the sum of the transverse momentum from all particles in event will be small.

4.3 Rapidity and Pseudorapidity

In non-relativistic physics velocity is additive which is useful for calculation. Unfortunately this does not apply in relativistic physics hence instead of velocity it is convinient to find a new variable representing a velocity which has additive character. This variable is rapidity.

$$y = \frac{1}{2} \ln \left(\tan \frac{E + p_z c}{E - p_z c} \right) \tag{4.5}$$

Lorentz transformation can be viewed as rotation through y representing an imaginary angle.

Not only momenta and energies of particles can be studied but what can bring us an interesting view of the collisions is also the geometry of the events. Space coordinates can be defined by azimuthal and polar angle ϕ, θ respectively. ϕ is measured in x, y plane but θ is measured from z direction which is along the beam. It is difficult to measure rapidity at high energies due to high z momentum component that is why observable pseudorapidity η is used instead

$$\eta = -\ln[\tan \frac{\theta}{2}] \tag{4.6}$$

From (4.6) can be seen that η depends only on the polar angle θ. When θ goes to zero rapidity goes to infinity. For high energies $\eta \simeq y$. As was discussed earlier detectors can't cover the whole area especially close to the tube which particles are moving through. Pseudorapidity is therefore also a good characteristics for detector acceptance.

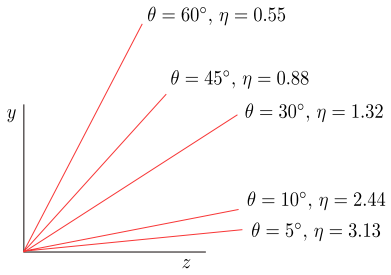

Fig. 4.1: Pseudorapidity for several values of polar angle ϕ.

4.4 Impact parameter

In some collisions particles collide directly towards each other ("head on" or central collision) in others particles only glance off each other and in the most cases they don't even cross over. This information about how close the particles was in interaction can be summarized by introducing impact parameter which is the distance between centers of two colliding proton.

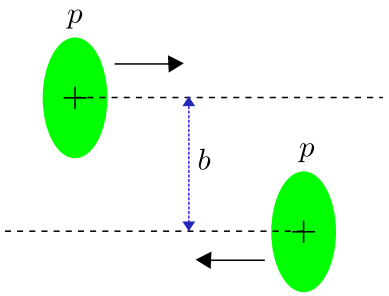

Fig. 4.2: Two colliding protons with the vertical impact parameter b.

4.5 Cross section

Cross section is a very common term in particle physics. To understand this term, firstly a standard simple case of beam and target will be introduced. Particles a shooted at a target with particles b don't move along a straight line rather in a beam hence their interaction with the target is at certain area A. From this interaction new particles c can be created flying away at a certain space angle Ω. In principle number of particles $\mathrm{d}N$ which impact on detector area dS between time interval t is what is experimentally measured and what eventualy leads to so far undescribed term cross section (Fig. 4.3).

$\mathrm{d}N$ depends on several terms. One of them is certainly how many particles will impact on the target area during the time interval t. In other words flux density j of particles a. The choice of target is important as well hence there is also dependence on number of particles b N_b which are impacted on. This is clearly $N_b = nV = nsA$ where n is a particle density, V volume in which particles are situated and which can be described as width d times already mentioned impacted area A. Two more things are remaining. Detector area $\mathrm{d}S$ which produced particles c are impacting on comes from space angle $\mathrm{d}\Omega$. The larger the Ω the larger the area $\mathrm{d}S$ leading to more c detecting. Lastly it is obvious that not every interaction can lead to creation of c therefore it is necessary to introduce the probability of interaction between particles a and b in which c will be created and will fly at a certain azimuthal and a polar angle ϕ, θ respectively. This probability is desired cross section $\sigma(\phi, \theta)$. As can be seen $\sigma(\phi, \theta)$ is an interesting probability because of its untraditional units m^2t^{-1}. Putting all terms together dN is given by

$$\mathrm{d}N(\phi, \theta) = jnsA\,\mathrm{d}\Omega\sigma(\phi, \theta). \tag{4.7}$$

From above equation σ can be separated

$$\sigma(\phi, \theta) \equiv \frac{\mathrm{d}\sigma}{\mathrm{d}\Omega} = \frac{\mathrm{d}N}{\mathrm{d}\Omega}\frac{1}{jnsA}. \tag{4.8}$$

Term $\frac{\mathrm{d}\sigma}{\mathrm{d}\Omega}$ is called differential cross section. For interest the dependance of differential cross section for Rutherford formula on scattering angle θ is given as following

$$\frac{\mathrm{d}\sigma}{\mathrm{d}\Omega} \propto \frac{1}{\sin^4\left(\frac{\theta}{2}\right)}. \tag{4.9}$$

Equation (4.8) is often written in a different form

$$\sigma(\phi, \theta) = \frac{R}{L}, \tag{4.10}$$

where $R = \mathrm{d}N/\mathrm{d}\Omega$ is called interaction rate (number of particles per sec) and $L = jnsA$ is luminosity. L is a constant dependant only on experiment. When integrated over time it has an area unit m^{-2}

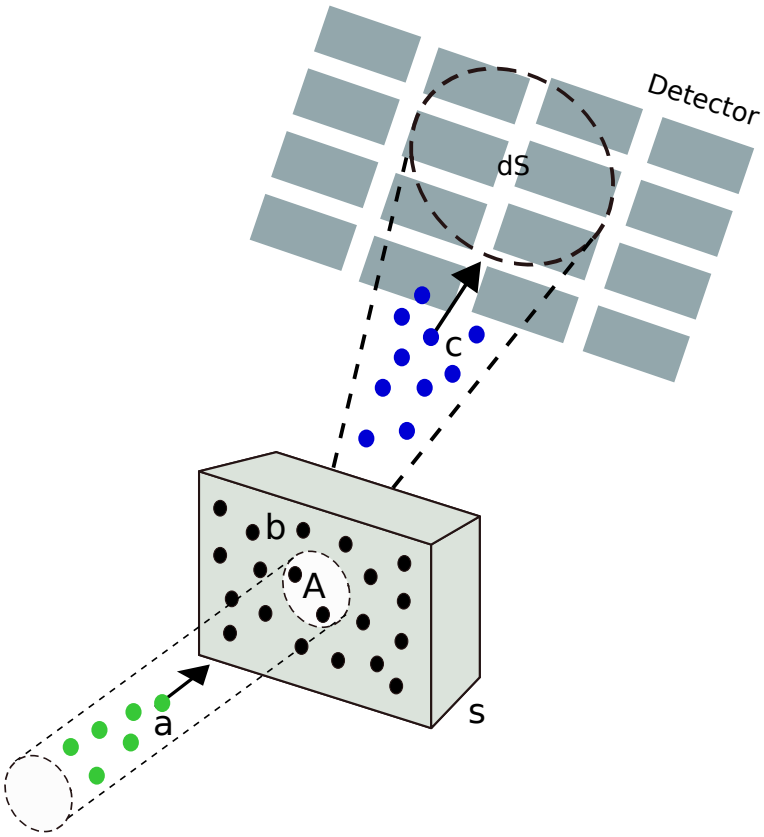

Fig. 4.3: Cartoon description of particles a impacting particles b in the target leading to creation of c which are later on detected.

but more often used are inverse barns b^{-1} ($1b = 10^{-28}m^2$), which is a large unit (for example the data presented in this thesis in Chapter 8 has integrated luminosity $169\mu b^{-1}$). Several aspects of particle physics such as spins of particle or the fact that proton has dynamic inner structure make σ much more complicated. For example cross section of interaction between two protons A and B can be written as following

$$\sigma_{AB} = \int \mathrm{d}x_a \, \mathrm{d}x_b f_{a/A}(x_a) f_{b/B}(x_b) \sigma_{ab\to X}, \tag{4.11}$$

x_a, x_b represent momenta fractions of parton (inner particle of proton) a from A proton, parton b from B proton and $f_{a/A}, f_{b/B}$ are partonic distribution functions. The last term $\sigma_{ab\to X}$ is probability of a interacting with b which results into creation of X.

Chapter 5

Inner structure of proton

5.1 Probing

To be able to see the inner structure a probe must have the wavelength λ which has the same or smaller value than the size of studied object (the same scenario as in microscopy). Theory of wave-particle duality says that there are cases when particle can be regarded as a regular particle which consists with understanding of classical mechanic but can also behave as a wave (interference images occur when particles are shooted through a slit). Therefore, the probe can be particle. The resolution of particle probe Δr is in consistancy with microscope resolution

$$\Delta r = \frac{\lambda}{\sin\theta}, \tag{5.1}$$

where λ is a wavelength of probe particle and θ is an angle of reffraction. Quantum theory gives an equation for energies $E = h\nu$ where h is planck constant and ν is a frequency. Applying this knowledge and wave-particle duality, the relationship between wavelength and momentum $\lambda = h/p$ can be derived. All together inserted into 5.1.

$$\Delta r = \frac{h}{p\sin\theta} = \frac{h}{q}, \tag{5.2}$$

where $q = p_f - p_i$ is a momentum transfer (p_f, p_i initial and final momentum respectively). It is clear that deeper structure can be studied with higher momentum transfer. The fact that protons have inner structure was in this way experimentaly proved through deep inelastic scattering (DIS) experiments of electrons off nucleus during the time $1967 - 1973$ in the Stanford Linear Accelerator Center [7] .

5.2 Bjorken Scalling

The cross section of electron scattering off protons can be written as following

$$\frac{d\sigma}{d\Omega} = \sigma_{mott}(W_2(\nu, q^2) + 2W_1(\nu, q^2)\tan^2\frac{\theta}{2}), \tag{5.3}$$

where σ_{mott} is basically the cross section for Rutherford scattering (4.9) formula with consideration of particles spins [22]. ν is the energy transfer $\nu = E_f - E_i$, E_i and E_f is the initial and final (before and after collision) energy of electron. θ is still the scattering angle and q is the momentum transfer. W_1, W_2 are nonelastic structure functions which represent how incoming electrons "see" the structure of the proton, and which needs to be parametrized. Björken proposed that this structure function will have scale behaviour for large q^2. The proper physical meaning of this scale behaviour will be better

introduced in following section-Parton model. It turned out that structure function for large q^2 can be written in a following form

$$2W_1 = \frac{Q^2}{2m^2}\delta(\nu - \frac{Q^2}{2m}), \tag{5.4}$$

$$W_2 = \delta(\nu - \frac{Q^2}{2m}), \tag{5.5}$$

and after substitution into (5.3) the cross section for DIS resembles elastic cross section. This can be viewed as electron interacting elasticaly with some point like objects which are inside the proton and have a mass m. Term $Q^2 = -q^2$ is introduced only for convinience (to have a better resemblance with elastic scattering formula). After multiplication (5.4) by m and getting ν out of the delta function, we will obtain the new form of structure functions which are only dependent on the ratio $x = Q^2/2m\nu$.

$$F_1(x) = 2mW_1 = x\delta(1-x) = \frac{Q^2}{2m\nu}\delta(1 - \frac{Q^2}{2m\nu}) \tag{5.6}$$

$$F_2 = \nu W_2 = \delta(1-x) = \delta(1 - \frac{Q^2}{2m\nu}) \tag{5.7}$$

where x is called Björken x scalling variable. As can be seen in Fig. 5.1 the elastic cross section falls off quickly whereas the cross section for DIS (at a given scale x) is decreasing slowly and in could be proclaimed as not dependant on Q^2. This (scaling) behaviour of structure functions at high momentum transfer was named "Björken scalling". However the DIS cross section is not clearly straight line. The reason behind this scalling violation lies in initial state radiation of partons (Chapter 6).

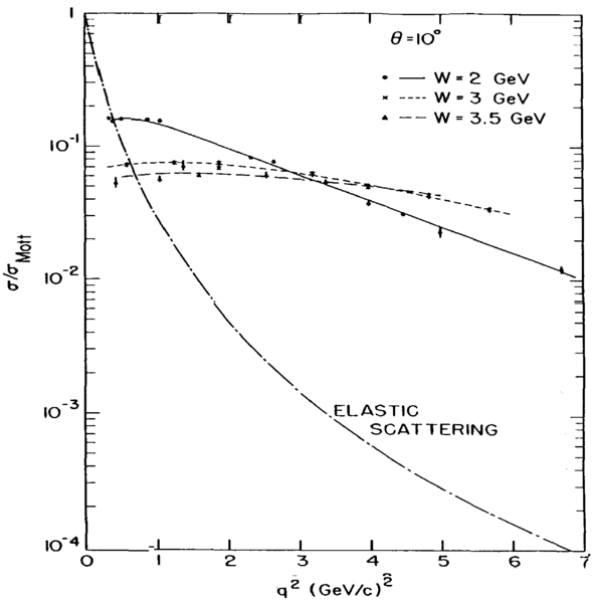

Fig. 5.1: Ratio of differential cross section σ and mott cross section σ_{mott} from (5.3) with respect to q^2 [9].

5.3 Parton model

The origin of Björken scalling was explained by Richard Feynman Parton model. As was introduced in section 5.1, higher Q^2 means that it is possible to look deeper into structure of object but it is not

true in Björken scalling therefore objects appear as points without additional inner structure. Parton model interpret this as electrons rebounding elasticaly from pointlike objects in proton. Feynman named these objects partons. This model consider infinite momentum frame where target proton is moving very fast. Assuming that proton is moving very fast with longitudial momentum p_L and negligible transverse momentum p_T, partons inside the proton moves almost collinear with the proton and each one of them is carrying some fraction of p_L. Quantum mechanics says that it is not possible to determine exactly how much momentum of the proton is carried by a particular parton but it is possible to predict a probability that parton is carrying certain amount of momentum. In this way parton distribution functions (PDFs) $f_i(x)$ are introduced and they represent probability densities to find i parton carrying the momentum fraction x. PDFs are related to structure functions through Callan-Gross relation [22]

$$2xF_1 = F_2 = \Sigma_i e_i^2 x f_i(x), \tag{5.8}$$

where e is an electric charge of parton and sum goes through all partons in the proton. Feynman introduced general term partons but as was already discussed in Chapter 2, it is known that there are quarks and gluons inside protons. In particular 3 valence quarks (uud), gluons holding them together and so called "sea quarks" representing virtual quark anti-quark pairs which are created when gluon splits and which anihilate with another quark with oposite charge. Values for PDFs are obtained through experiments (Fig. 5.2) and depends on Q^2. The structure of proton is parametrized at some Q_0^2. PDFs are extracted by using theory to evolve the structure from Q_0^2 to Q^2 of the actual collision.

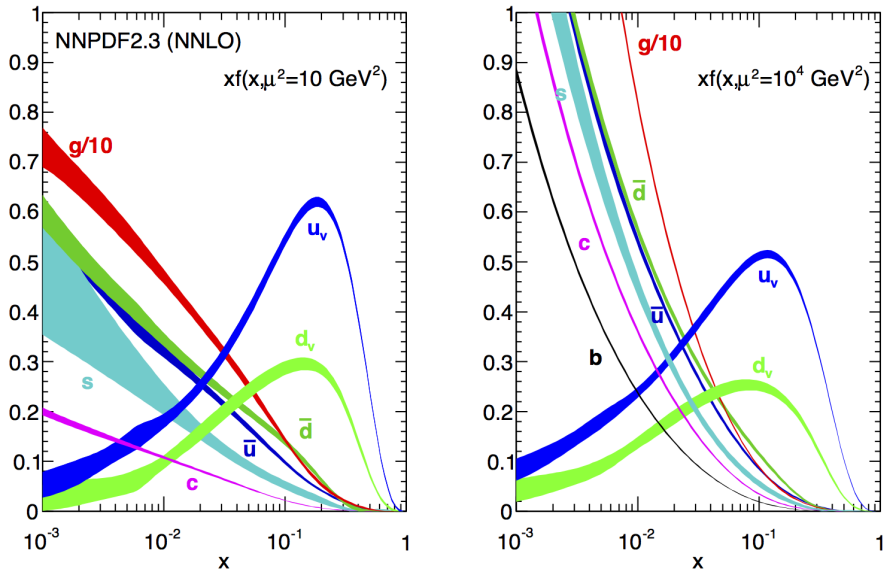

Fig. 5.2: Parton distribution function for u, $\bar{u}$, d, $\bar{d}$, c, s, b quarks and gluon (divided by 10) at two different Q^2 with respect to momentum fraction x [8].

Chapter 6

Theory of pp collisions in MC

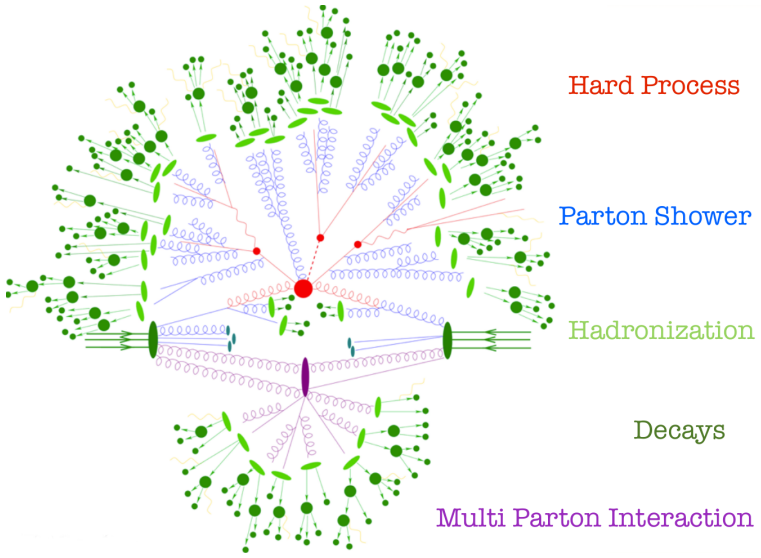

Fig. 6.1: Simulation of *pp* collision by MC method [19]. Individual colours are representing different processes according to the colour of the text on the right.

Theory of pp collisions comes in a few main steps (Fig. 6.1) and eventually leads to complicated multidimensional integrals which are solved by MC method (usage of MC generators). The hard process with the high momentum transfer between partons is at the core of simulating collision and it's cross section is calculable from PDFs (4.11). Partons are colour charged objects and in an analogue with radiation of electricaly charged particles, they can radiate gluons when traveling through an external field. This evolution of incoming and outgoing partons is described by parton showers. Because partons are objects which feel the strong interaction they are confined to the composite objects through process called hadronization. Two additional processes take place in generating events. Multiparton interaction and decay. The first one is an effect of composite structure of protons and means that more than one parton can interact with partons from other proton. Not all particles are stable and because of their heavy mass they decay into other particles which can be later on seen in the detector.

6.1 Parton showers

When electrically charged particle is scattered it radiates a photon. In a similar way gluons are radiated through scattering of particle with colour charge. Gluons also carry colour charge unlike photons therefore gluons can itself be sources of another gluon radiation eventualy forming a cascade Fig. 6.2. The radiation is possible before (Initial state radiation-ISR) and after the interaction (Final state radiation-FSR). Both ISR and FSR use the same main idea but differs in some aspects. The

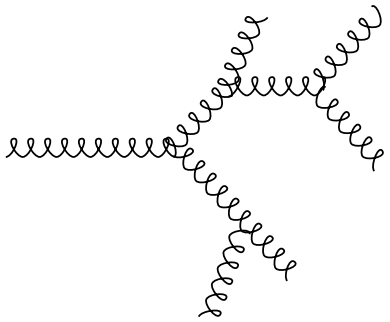

Fig. 6.2: Gluon radiating cascade.

starting point is the DGLAP (Dokshitzer, Gribov, Lipatov, Altarelli and Parisi) equation (6.1) [11] giving a probability that a parton a will branch into partons b and c at some scale t.

$$\mathrm{d}P_a(z,t) = \frac{\mathrm{d}t}{t}\frac{\alpha_s}{2\pi}P_{a\to bc}(z)dz \tag{6.1}$$

Square of transverse momentum p_T^2 or virtuality Q^2 which represents momentum transfer are often used as a choice for the scale. z is the fraction of energy of a taken by b hence parton c takes away $(1-z)$. $P_{a\to bc}$ is the splitting kernels and its form depends on the process ($q \to qg$, $g \to gg$, $g \to q\bar{q}$). So far the emission probability distribution from (6.1) is presented for all inclusive gluons meaning that their total energy is the total energy of all emited gluons. It is convinient to introduce ordering variable (for example p_T^2) and obtain only some exclusive gluons with emission probability of parton between p_T^2 and $p_T^2 + \mathrm{d}p_T^2$. This idea can be implemented into emission probability through Sudakov form factor [23]

$$\Delta(p_{Tmax}^2, p_T^2) = \exp\left(-\int\int \mathrm{d}P_a(z\prime, p_T^2\prime)\right). \tag{6.2}$$

In other words probability of no emission between p_{Tmax}^2 and p_T^2. Combining all together the overall emission probability is given by

$$\mathrm{d}P_a = \frac{\mathrm{d}p_T^2}{p_T^2}\frac{\alpha_s(p_T^2)}{2\pi}P_{a\to bc}(z)dz\Delta(p_{Tmax}^2, p_T^2). \tag{6.3}$$

In FSR the hard process was already chosen (given p_{Tmax}^2, or Q^2,...) and the evolution started from that point going to lower values till $\sim$ 1GeV where hadronization takes place. In case of ISR it could be done the same way and it is possible to try to get to the chosen hard process, however, this procedure is highly inefficient. It would require generating a vast amount of processes from starting point, where partons are going into interaction and are radiating on the way, but only a few of these generated processes would get to a sufficient x. It is more convinient to start from hard interaction and do backward evolution. In this way the question is not what is the probability of parton a emission $\mathrm{d}P_a$ but rather the probability that parton b was radiated from parton a which has a certain distribution f_a.

$$\mathrm{d}P_b = \frac{\mathrm{d}p_T^2}{p_T^2}\frac{x\prime f_a(x\prime, p_T^2)}{x f_b(x, p_T^2)}\frac{\alpha_s(p_T^2)}{2\pi}P_{a\to bc}(z)dz\Delta(x, p_{Tmax}^2, p_T^2) \tag{6.4}$$

Both probabilities in question (6.3) and (6.4) bear resemblance except the term with ratio of parton densities where in denominator there is a PDFs for current parton b with its value of x and in nominator values for new parton a which b can evolve to. This new term is also included in Sudakov form factor.

6.2 Hadronization

So far everything was discussed on parton level - hard process which was introduced as high momentum transfer between **partons**, **parton** shower, multi-**parton** interaction, however what is detected and measured are not partons but hadrons. Therefore there has to be a process between creating individual partons and measuring hadrons (Hadronization) which requires theoretical description. String model and Cluster model are todays main approaches to describe this phenomena. Due to the effect of asymptotic freedom the interaction between charges in QCD is quite different from the case in QED (Fig. 6.3). As colour charges are travelling away from each other the potential between them is linearly

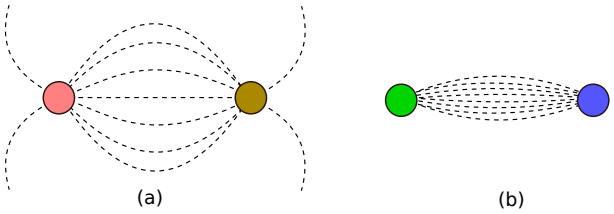

Fig. 6.3: Field lines in QED (a) and QCD (b) between charge and anticharge.

rising, similar to the potential of a string kx where k is a string constant and x a distance. To separate them an infinite amount of energy have to be supplied. String tension κ (constant similar to k) can be obtained from hadron spectroscopy and was found to be roughly $\kappa \approx 1$ GeV/fm. The first step of

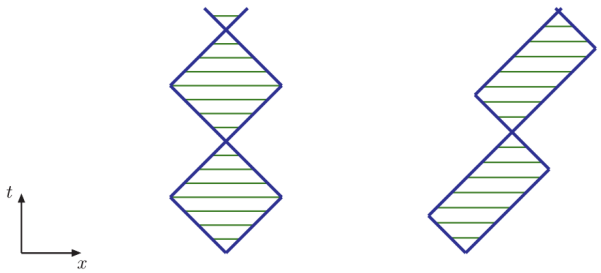

Fig. 6.4: Cartoon of string (between quark and anti-quark) behaviour in time and along x-axis in the CMS frame (a) and in the boosted frame (b) [12].

the string model is the following. When at some point in time and space $q\bar{q}$ are flying from each other, string stretches among them creating a constant tension κ. As they move from each other, they reach a point where the kinetic energy of quarks won't be sufficient to overcome potential from the string and quarks start to accelerate towards each other, meeting back at the starting point and the whole process starts over. In Fig. 6.4 there are two cartoons symbolizing development of the string in time and along x-axis in the different frames. The left figure is in the CMS frame which is the reason why the cartoon looks symetric and the right is in the boosted frame. In the boosted frame the point of

reversion is not simultaneous which is the reason why the second cartoon looks tilted, however the area of rectangulars is the same, therefore Lorentz invariant. It can occur that string will break leading to string fragmentation. It is possible for additional $q\bar{q}$ pair to tunnel out of the vacuum and these two new quarks can be attached to the initial string breaking it into two strings. Fragmentation can happen all the way along the string hence more hadrons can be created. The disconnection of string

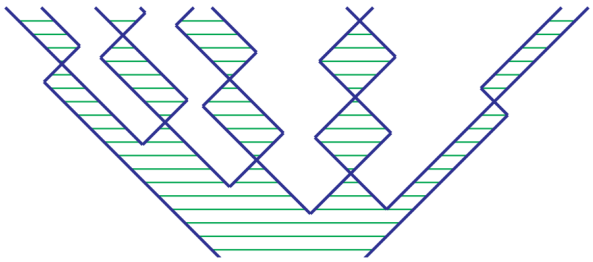

Fig. 6.5: Cartoon of string fragmentation [12].

happens in a way that the two branches "don't know" about each other (don't depend on history between them → acausality) and it is possible to describe the process from both ways (either from q or $\bar{q}$).

Interesting feature is with a three parton system $q\bar{q}g$. Particles are colour connected → quark colour charge with gluon anti-colour charge and gluon charge with anti-charge of anti-quark. Hadrons will

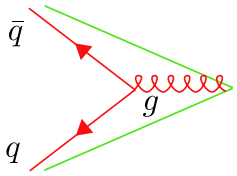

Fig. 6.6: String structure between $q\bar{q}g$.

be created preferentially in the way of partons motions because of the boost character. Most hadrons will go between the quark gluon segment and gluon anti-quark segment and only a few to the quark anti-quark. This string effect was experimentally proved by comparing 3-jet events to 2-jet + photon events at the PETRA and LEP experiments.

In the cluster model every gluon from parton shower is splitted into $q\bar{q}$ pair. Clusters ,the basic units of the method, are colourless objects composed of $q\bar{q}\prime$. $\bar{q}\prime$ is anti-quark from different brach which needs to be colour matched to the q, therefore it is necessary to know the colour of every parton. This track keeping of colour flow through event is called preconfinement. It turns out that for most of the cases q are paired with $\bar{q}\prime$ from adjecent branch Fig. 6.7. Clusters decay into lighter resonannces and stable hadrons.
Whereas the string model is more economical in energy-momentum picture (needs less parameters for description) the cluster model is far better in flavour correlation.

6.3 Decays

Between hadronization and measuring hadrons actually one other process takes place and that is particle decay. Hadronization and decay process are highly connected and tuned parameters for hadronization is applicable only with particular decay package hence these procedures go hand by hand. A lot

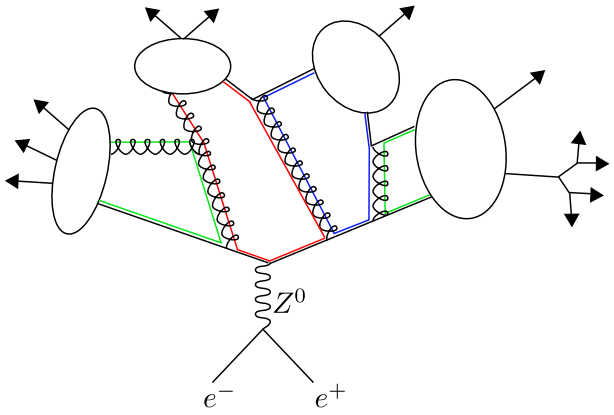

Fig. 6.7: Cartoon of cluster model with preconfinment.

of decays have been measured and noted to Particle data group (PDG) review of particle physics, however not all of them (heavy quark baryons, excited meson multiplet, ...).

6.4 Multiparton Interactions (MPI)

In section 4.5 the concept of cross section was introduced. However, theory needs to be proved by experiment. It is not possible to calculate the total cross section ($\sigma_{tot} = \sigma_{elastic} + \sigma_{ND} + \sigma_{SD} + \sigma_{DD}$) from the formula, only the hard cross section where perturbative QCD is applicable. For that reason only calculable hard cross section and experimentaly measured cross section are compared in Fig. 6.8. Because the hard cross section diverges when $p_T \to 0$ it is necessary to aply a cut and integrate the

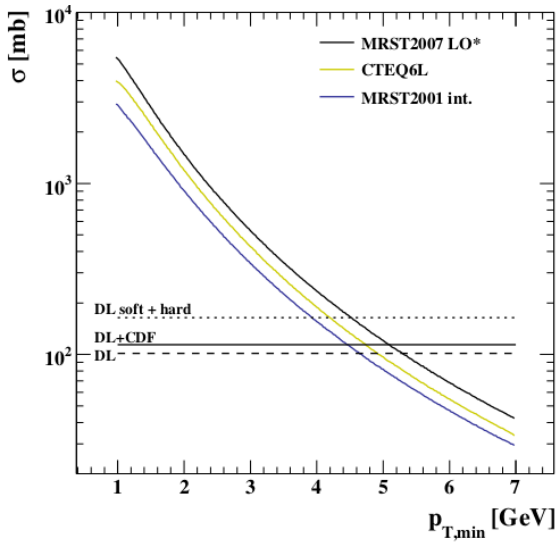

Fig. 6.8: Comparison between inclusive $2 \to 2$ hard cross section for three different PDFs and various DL (Donnachie Landshoff) extrapolation of the non-perturbative fits to the pp cross section at $\sqrt{s}$= 14 TeV from CDF experiment [13].

cross section from some $p_{T,min}$ which is going to be a parameter to be fitted. The result of the com-

parison is a bit unexpected.

The hard cross section should be embeded in the total cross section, which is however exceeded by hard cross section. It is like the probability beeing hit by a truck (hard process) is larger than beeing hit by any vehicle including the truck. The reason lies in multi parton interaction. As was discussed in chapter 5 there are quarks and gluons inside each proton and the idea is that not only partons with the highest momentum fraction can interact but also other partons are able to undergo interaction with parton from other proton. Hard cross section is an inclusive number so if there are two interactions it counts twice in hard cross section but only once in the total cross section. Because of this aspect the hard cross section eventualy overcomes the total cross section. To prove this idea of MPI several models were constructed and implemented into MC generators. One example is Sjöstrand-Zijl MPI model [24] introduced in 1987 which aimed to describe multiplicities of charged particle distribution at the data from UA5. The assumption of the model is that the mean number of interaction $\langle n \rangle$ can be introduced as following

$$\langle n \rangle (p_{Tmin}) = \frac{\sigma_{hard}(p_{Tmin})}{\sigma_{tot}} \approx \frac{\sigma_{hard}(p_{Tmin})}{\sigma_{ND}}. \tag{6.5}$$

The approximation to σ_{ND} in the previous equation comes from experiment and is used because of convenience (ND represents major contribution to events). At the beginning of this chapter it was mentioned that the cross section diverges when $p_T \to 0$ and hence the cutoff $p_{T,min}$ was applied. Sjöstrand-Zijl model handels this divergence with regularization factor which has theoretical background in colour screening (Fig. 6.9).

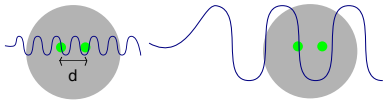

Fig. 6.9: Two partons separated in a proton by length d viewed by a gluon with two different wave lengths.

The Approximation of perturbative cross section is that particles are incoming in free states and thus it does not consider confinement of partons. But the partons can be affected by other partons in particulary it can occur that the colour charge of parton can be screened by it's anti-charge. When strongly interacting gluon has a wave length which is larger than the typical charge separation d, it can no longer resolve charges separably which leads to a reduced effective coupling. The perturbative cross section is divergent as $\alpha_s^2(p_T^2)/p_T^4$ therefore it is multiplied by a regularization factor

$$\frac{\alpha_s^2(p_{T0}^2 + p_T^2)}{\alpha_s^2(p_T^2)} \frac{p_T^4}{(p_{T0}^2 + p_T^2)^2}, \tag{6.6}$$

where p_{T0} represents free parameter which has an energy dependance and has to be tuned.
The model is also dependent on impact parameter b. The time integrated overlap of incoming hadrons at impact parameter b during collision (representing how central was the collision) is given by

$$O = \int \mathrm{d}t \int \mathrm{d}^3x \rho(x,y,z)\rho(x,y,z-\sqrt{b^2+t^2}), \tag{6.7}$$

where ρ represents matter distribution after a scale change because of relativistic effects. The more protons overlap the more interactions are expected hence the mean number of iteraction $\langle n \rangle$ is proportional to the overlap O. This idea describes quite well the "pedestal effect" Fig. 6.10. The transverse region is perpendicular to hard scattering thus contain mainly UE activity. The Fig. 6.10 shows that

with rising transverse momenta of objects from hard scattering there is minimal change in number of particles in the transverse region. MPI represent the most part of the UE activity in the transverse region. Therefore, it can be assumed that there is no change in MPI behaviour with rising p_T of objects from hard scattering and thus the collisions are central (because of MPI dependence on O). The description of MC (Fig. 6.11, Fig. 6.12) is clearly not perfect but it is obviously that after MPI

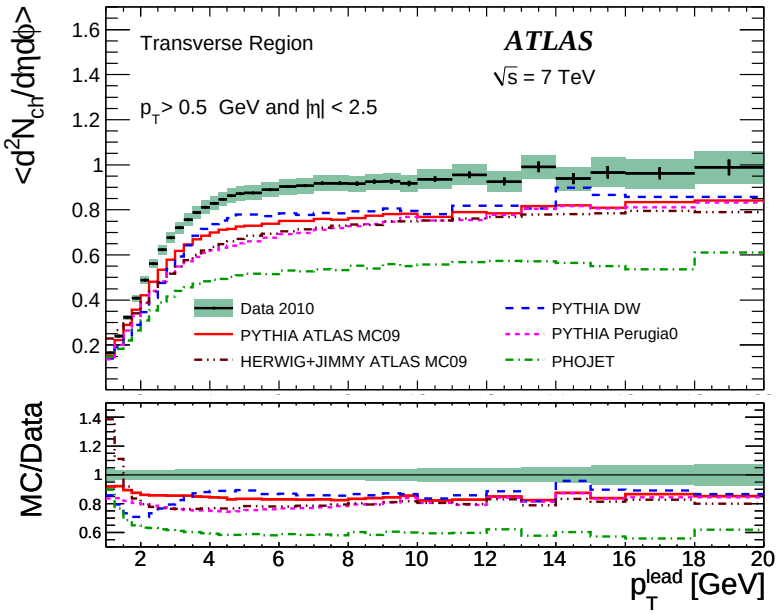

Fig. 6.10: Mean number of stable charged particles per unit η and azimuthal angle ϕ in transverse region (definition of regions in chapter 8) with respect to the highest p_T from the event [4].

implementation (right figure), MC better fits the data than without MPI (left figure) thus the idea of MPI is the right step towards better understanding of the non-perturbative QCD.
Except for better describing the data with MPI models there is also other way, which is maybe more obvious, how to prove the existence of MPI. For example by studying events with four jets and correlations between jet angles. Except the double Bremsstrahlung scattering (DBS) coming from single parton scattering where the angles are correlated it is possible to find subsample of so called double parton scattering (DBS) in which there is no correlation.

Complete understanding of MPI is still not near the end but current aproach is definetely not stagnating. New improvements are being invented and implemented into the MC models. For example the model of rescattering with the idea of additional scattering [14] or MPI with x-dependent proton size [15].

6.5 Monte Carlo models

Pythia8

The total inelastic cross section in Pythia8 is separated into non-diffractive and diffractive processes. The exchange of gluon between two coloured objects represents the dominant part of non-diffractive processes and its simulation includes multiple parton-parton inter- actions (MPI). The diffractive part

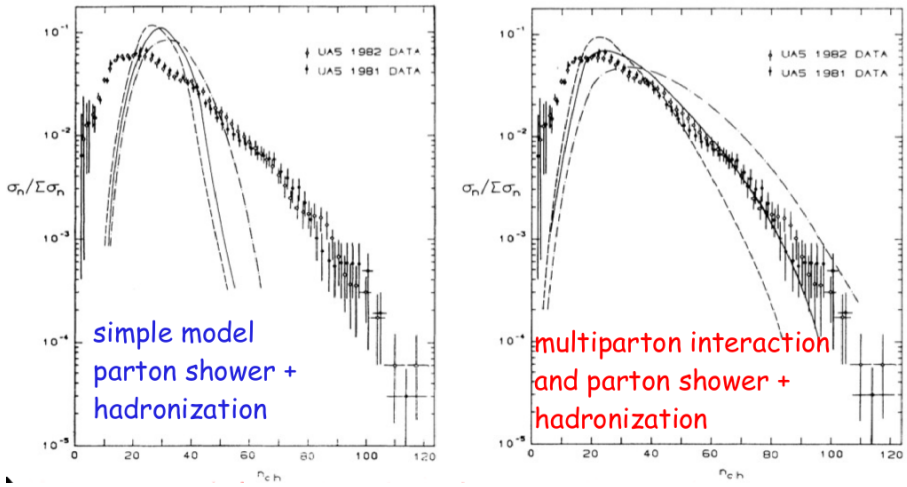

Fig. 6.11: UA5 Measurement of charged particle multiplicities. Dots are representing the data and dashed lines MC [10].

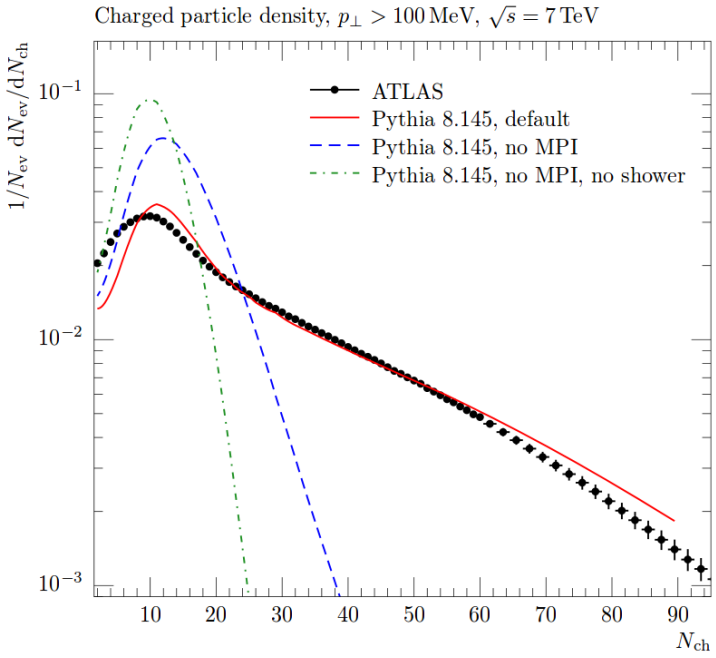

Fig. 6.12: Comparison of Pythia (with and without MPI and shower models turned on) and the data taken by the ATLAS [20]. Measured observable is charged particle multiplicity in events with particles satisfying following criteria → $p_T > 100$ MeV, $|\eta| < 2.5$, $c\tau < 10$ mm. At least two particles passing the criteria was required to consider the event [21]

is further divided into single-diffractive dissociation (SD) and double-diffractive dissociation (DD) which was introduced in Chapter 3. This thesis compares data with two Pythia8 tunes. The first one is the ATLAS minimum-bias tune A2 [26] (based on the MSTW2008LO PDF) which is good at

describing minimum bias events. The other one is Monash [29] (NNPDF2.3LO PDF) which among others uses and underlying-event data from the LHC at 7 TeV to constrain ISR and MPI parameters.

Herwig++

Unlike Pythia8, Herwig++ does not have a diffractive components. The MPI model for the non-diffractive processes is applied to events where there is no hard scattering. This leads to possibility of simulating the event with zero $2 \to 2$ scattering. Herwig version 2.7.1 (CTEQ6L1 PDF) is used with a 7 TeV underlying event tune UE-EE-5-CTEQ6 [28].

Chapter 7

Detector ATLAS and the LHC

The size of proton is approximately 10^{-15} m therefore it is complicated to collide them. To raise the chances of collisions, instead of colliding protons, the LHC collides bunches of protons. There will be bunches circulating in the beam pipe with the 25 ns difference between them at the nominal condition at the LHC at 13 TeV. Each bunch will contain 120 bilion of protons [31]. However even if particles collide it is not possible to see the collision with the naked eye. There are four main detectors distributed around the LHC with the vast amount of electronics to measure particles going from collisions and one of these detectors is The ATLAS (**A** **T**oroidal **L**HC **A**pparatu**S**). Its purpose is to experimentaly study physics within the SM (Higgs boson) and beyond (Supersymmetry). The whole ATLAS detector is depicted in Fig. 7.1.

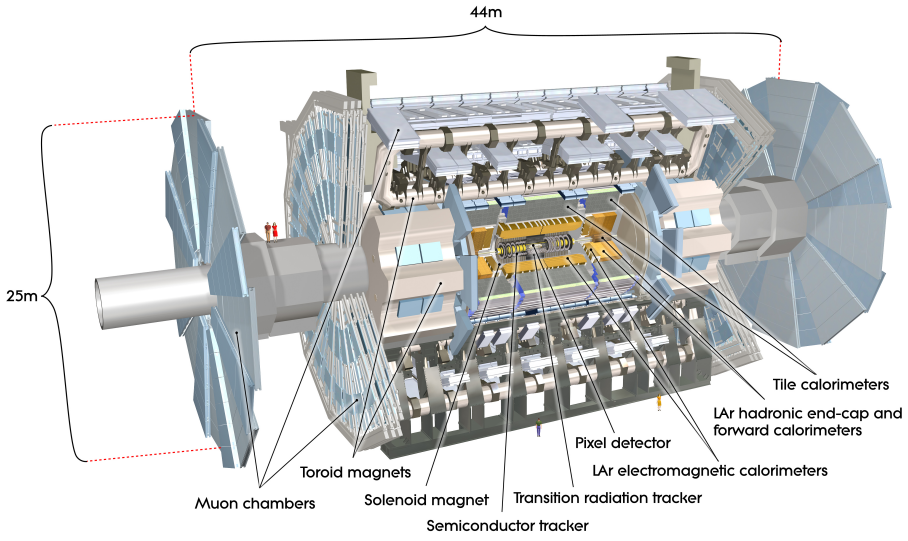

Fig. 7.1: The ATLAS detector and its part [16].

7.1 ATLAS detector subsystems

The ATLAS detector has 4 main parts → Inner detector (ID), calorimeters, muon chambers and magnet system. Calorimeter's purpose is to measure the energy of particles by absorbing them. Muon chambers are necassary to measure highly penetrable particles as muons. Magnets curve the paths of charged particles through detector due to Lorentz force which is proportional to particle velocity. In this way particle momentum can be measured.

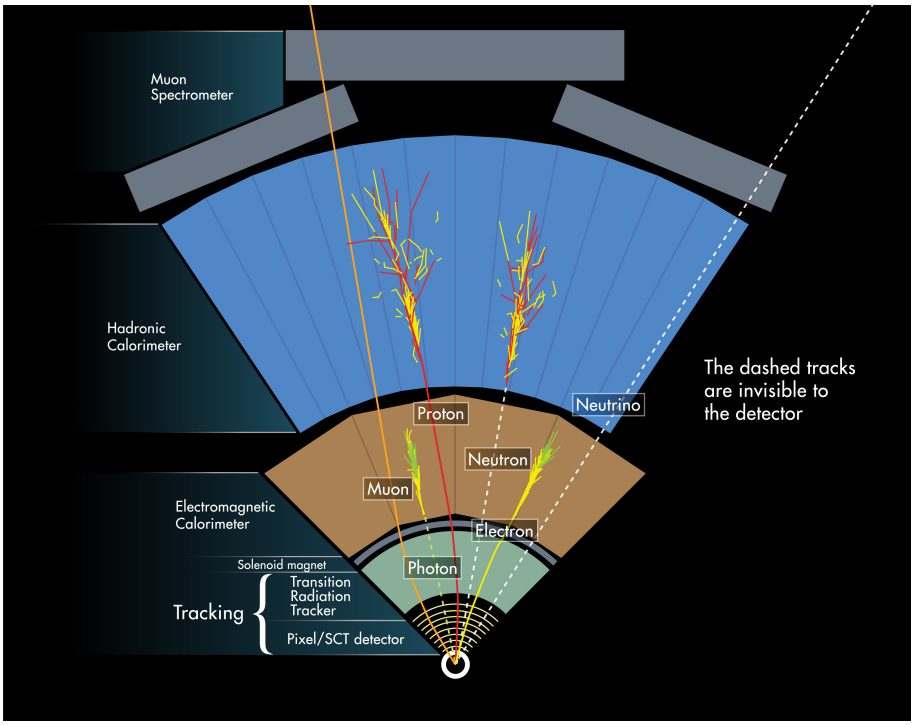

Fig. 7.2: Propagation of particles through layers of the ATLAS detector [17].

The inner detector, which is the closest to the beam pipe, is the most important part for this thesis because it is this part that allows for the track reconstruction ("tracking"). As particles move from the collision they hit layers of the detector. To combine these hits from all the sublayers of ID and to create a path/track of propagating particle is what is called tracking and is based on various algorithm.

The ID is additionaly subdivided into Pixel, Semiconducter tracker (SCT) and Transition radiation tracker (TRT) situated respectively from the beam pipe. Each one of them has several layers and their geometry around the beam pipe is in form of barrel and end-caps. End-caps are discs around the beam pipe with detectors placed on the surface of the discs. Due to this combination of barrel and end-caps it is possible to better detect particles flying from collision. More detailed description of ID can be found in [18].

During the last upgrade of the LHC and ATLAS, the new Insertable B-layer (IBL) detector was installed [25]. This layer is placed between the Pixel and the new beam pipe which has a smaller radius than the previous one. The LHC is aiming for higher luminosities, but design of Pixel is not sufficient

and would lead to degradation of tracking. To prevent that is one of purposes of the IBL.

7.2 Trigger system

It is not technically possible to record the data from all collisions. Unfortunately the average event rate needs to be reduced from 40 MHz (which is the expected collision rate at 13 TeV when the distance between bunches is 25 ns) to 1 kHz which is the limit of storage rate in Run II. Therefore a lot of events have to be thrown away. To perform this task ATLAS has a trigger system which combines hardware and software to record only events which are for some reason interresting. The ATLAS trigger system comes in three levels → level 1 (L1), level 2 (L2) and Event Filter (EF). To pass each level events have to complete certain criteria (for example requirement on hits in a certain part of detector) only after that they are selected.

Especially important part of the Trigger system for this measurement is Minimum Bias Trigger Scintilator (MBTS). The term Minimum bias (MB) refers to as little constraint for events as possible. MB events contain typically low p_T particles coming mainly from ND collisions. Coverage of pseudorapidity for MBTS in Run II is for inner ring $2.76 < |\eta| < 3.86$ and for the outer ring $2.08 < |\eta| < 2.76$. The MBTS is important for these soft inclusive events as well as for the UE due to their close relation.

7.3 Reconstruction

In Fig. 7.3 there is an approximation of event evolution in time which can be divided into parton, particle and detector level. Taking the first one aside, the effort is to measure the particle level. Unfortunately, the only observable part in real data is at the detector level. MCs such as Pythia on the other hand can generate things on particle level (particle on particle level does not sound well hence are rather refered as truth) and by running the results from particle level through simulations (for example Geant) the final detector level (in this case particle is refered as track) can be obtained. The advantage of this MC approach is presented in paragraphs below.

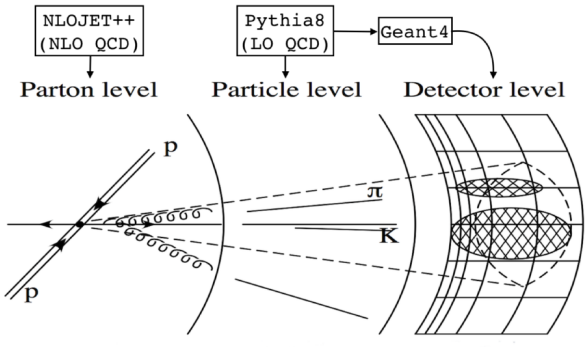

Fig. 7.3: Event evolution with parton, particle and detector level [32]

Track reconstruction is a process in which particle trajectories through detector are reconstructed. Not every track is reconstructed as it should be, connecting hits in detector which does not belong to same particle (fake tracks). Some tracks are even not recostructed at all and are lost from events. Track

reconstruction has therefore its efficiency which depends on p_T and η of track. Points in space where collisions take place are reconstructed as well. These points are called vertices and their reconstruction efficiency also varies.

The reconstruction takes place between particle and detector level. Needless to say that to obtain particle level it is necassary to go backward through reconstruction, which is done by applying corrections including mentioned efficiencies to data.

Reconstruction efficiencies can be acquired from MC, because from MC point of view observables for example the number of particles are known on both particle and detector level therefore by comparing them the loss of particles can be gained. However, reconstruction efficiency has to be obviously independent on the model of MC. At this point it is good to mention matching procedure which is done to match a track with its truth particle. The procedure is done through hit based matching algorithm which compares number of shared hits in detectors between track and truth.

In Chapter 8 there are several selection criteria concerning reconstruction as requirements for impact parameters. Transverse impact parameter b was already introduced in chapter Variables but only for pp collision. The definition of new longitudial impact parameter z_0 and also transverse d_0 is best explained through Fig. 7.4. Both parameters are with respect to the origin O which is fixed. However these parameters can be also taken with respect to the beam line which is described as the luminous region produced by the collision of proton beams. If there is a multi proton-proton interaction (more

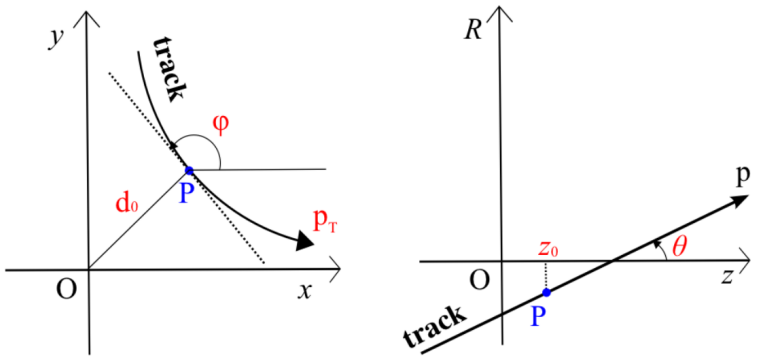

Fig. 7.4: Description of longitudial impact parameter z_0 and transverse impact parameter b_0. Left picture is a track projection to xy plane and right picture track projection to Rz plane. P denotes point of the closest approach to the plane [18].

than one pp interaction) then event is said to have a pile-up. In many cases pile-up is unwanted effect because instead of studying interaction it brings mix of interactions. As pile-up means more interaction, more vertices can be reconstructed, however contribution of events with this effect can be reduced by suitable selection of events leaving only primary vertex which is the vertex with the highest sum of tracks p_T^2. In reconstruction process path of the track is fitted to the detector hits. How good the fit is describes the χ^2 distribution. In principle the values of fit and hits (position) are squared and sum up and if the result is above certain determined value the track can be rejected.

Chapter 8

Analysis

It is important to know the comparison of MC models with data as soon as possible before generating a vast amount of events. The aim of this measurement is to provide ATLAS collaboration with this very quick comparison for which the detector level is sufficient. Nevertheless the selection criteria for particle level and correction procedure are also mentioned because the next step of this analysis will be exactly correction to particle level in order to be able to publish the data.

The particles of interest are primary charged particles defined as charged particles with a mean proper lifetime $\tau_{prim} \gtrsim 0.3 \cdot 10^{-10}$ s. This includes either particles coming directly from the collision or particles which decayed from the ones with $\tau < \tau_{prim}$. The truth-track notation introduced in Section 7.3 will be held. As was mentioned in Chapter 1, the UE activity is studied in three regions toward, transverse and away. These regions are defined by finding a track with the highest p_T henceforth called leading track. By measuring the azimuthal angle $\Delta\phi = \phi - \phi_{lead}$ from leading track ϕ_{lead} the xy plane can be divided as shown in the Fig. 8.1.

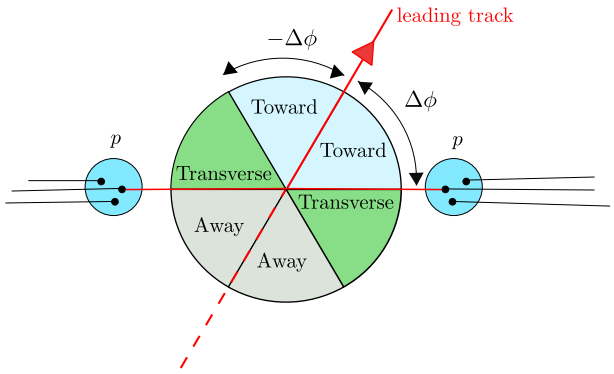

Fig. 8.1: Collision where the hardest object is taken as the leading track from which the xy plane is divided into regions.

- Toward region $|\Delta\phi| < \pi/3$
- Transverse region $\pi/3 < |\Delta\phi| < 2\pi/3$
- Away region $2\pi/3 < |\Delta\phi|$

Contribution of the UE differs from region to region. For example the MPI is the main component in the transverse region. On the other hand parton showers are produced more likely in the vicinity

of high energy tracks/particles therefore in toward and away region (nevertheless can also accompany hard particle from MPI in transverse). Due to the effect of this UE components, jets show more activity.

All observables of this measurement can be found in Tab 8.1. The choice of observables is mainly to reflect collective behaviour of particles in an event.

	$\langle \mathrm{d}^2 N_{ch}/\,\mathrm{d}\eta\,\mathrm{d}\phi \rangle$	$\langle \mathrm{d}^2 \Sigma p_T/\,\mathrm{d}\eta\,\mathrm{d}\phi \rangle$	$\langle p_T \rangle$
Particle level	Mean number of stable charged particles per unit $\eta\phi$	Mean scalar p_T sum of stable charged particles per unit $\eta\phi$	average p_T of stable charges particles
Detector level	Mean number of selected tracks per unit $\eta\phi$	Mean scalar p_T sum of selected tracks per unit $\eta\phi$	average p_T of selected tracks

Tab. 8.1: Measured observables on detector and particle level.

8.1 Selection criteria

The data presented in this thesis are combination from the ATLAS run-267358 and run-267359 in Run II. The first fill was taken on the 10th June from 00:20 till 02:05 and has a very low pile up $\mu = 0.3\%$. Number of events in Fill1 is 8,665,704. The second fill was taken on the same day between 05:41 and 07:50. The pile up was $\mu = 0.7\%$ and the number of events 12,295,654. Only the data from GoodRunList (GRL), representing the high-quality data for this analysis, was used. The trigger selection was done by HLT_noalg_mb_L1MBTS_1 which requires at least one hit in either of the MBTS scintillators on either side of ATLAS. Either events with primary vertex or primary vertex with secondary which has number of tracks ≤ 4 were considered. Other events were rejected in order to remove pile-up events.

To be considered in the event, tracks has to pass following criteria:

- $|d_0| < 1.5$ mm
- $|z_0 - v_Z| \sin\theta < 1.5$ mm
- $|\eta| \leq 2.5$
- $p_T > 500$ MeV
- if IBL hit is expected than at least 1 hit is required if not than at least 1 hit in Layer-0 (Pixel first layer) expected
- at least 1 pixel hit + dead sensors
- at least 6 SCT hits + dead sensors
- if $p_T > 10$ GeV than requirement $\chi^2 < 0.01$

The condition on particle level are presented below

- Only primary particles (strange baryons excluded, explanation in Section 8.3)

- $p_T > 500$ MeV
- $|\eta| < 2.5$

The particle level is important for correction procedure (section 8.3) which is additional step after detector level plots) but is not included in this thesis.

Because of the close relation with the MB measurement [33] the selection criteria are the same except the condition on the leading track with $p_T^{lead} > 1$ GeV. The p_T^{lead} cut reduces contribution of diffractive interaction leaving non diffractive events as the dominant part (comparison of ND,SD,DD components for Monash is depicted in Fig. 8.2). In addition, condition on p_T^{lead} also leads to trigger and vertex reconstruction to be almost fully efficient.

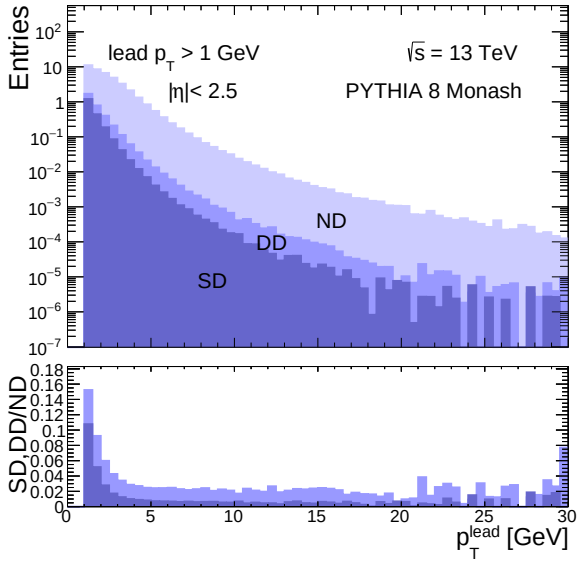

Fig. 8.2: Comparison of Monash non-difractive, double difractive and single difractive p_T^{lead} components

The total number of triggered events in the data and the number after several p_T^{lead} cuts are in the Tab 8.2.

Trig. Events	p_T^{lead} >1GeV	p_T^{lead} >3GeV	p_T^{lead} >5GeV	p_T^{lead} >10GeV
≈ 1.3e+07	≈ 7.6e+06	≈ 1.4e+06	≈ 2.8e+05	≈ 2.1e+04

Tab. 8.2: Number of triggered events and events with $p_T^{lead} > 1$,3,5 and 10 GeV.

8.2 Results

The data are compared with MC generators Pythia8 A2, Pythia8 Monash and Herwig++ on the detector level as mentioned. A2 is ATLAS minimum bias tune based on previous results including Run I. Therefore, it is expected that it would describe data better at lower p_T. On the other hand, both Pythia8 Monash and Herwig++ have higher weights on UE observables.

8.2.1 Multiplicities

N_{ch} **vs** $|\Delta\phi|$

In Fig. 8.3 there are the mean numbers of tracks in event (termed as multiplicity) with respect to $|\Delta\phi|$ for different p_T^{lead} cuts. Multiplicity is normalized to the unit in eta phi space. Therefore, it is divided by 5 (for η between -2.5 and 2.5) then by 2 (for $|\Delta\phi|$) and by width of bins. The leading track was excluded from all four histograms because of the better depiction, otherwise the value at $|\Delta\phi| = 0$ would stand out too much from other values. Multiplicity is the highest in the toward region. Then it drops down in the transverse region where it hits the minimum (for the data at around 1.2) and rising again in the away region. This character can be seen for all four histograms. At $p_T^{lead} >$ 5GeV the area between 0.8 and 1.6 (part of transverse region) starts to form a plateau which is called underlying event pedestal. This pedestal is even more visible later on in Fig. 8.4.
For $p_T^{lead} > 1$ GeV the MCs are not describing the data in toward region well. The difference is around 20 % for Monash and 15 % for A2 even Herwig which describes the first half of the toward region quite well starts to pull away from the data. A2 and Monash are also overshooting the data in the away region where the difference is the highest for Monash at around 10 %. The Transverse region is described much better with A2 where the difference is below 5%. With rising p_T^{lead} cut the situation changes and both Monash and Herwig start to describe the Transverse region better than A2 which is moving away from the data. From 5 GeV the difference between Monash and data or Herwig and data in transverse region is only a few % and the picture does not seem to break even at higher p_T^{lead}.

N_{ch} **vs** p_T^{lead}

Mean number of tracks with respect to p_T^{lead} is in Fig. 8.4. In this case the mean number of tracks is divided by $5 \cdot 2/3 \cdot \pi$ where $2/3\pi$ is the size of each region (toward, transverse, away). Steep rise can be seen in all regions between 1 and 5 GeV. The mean number of tracks is then slowly rising in both toward and away regions. In away region there are even more tracks than in toward because most of the energy is carried by leading track whereas in away, the energy is more distributed between tracks which leads to creation of more particles. On the other hand, particle density in Transverse is from 5 GeV almost flat. This is already mentioned UE pedestal. Its origin is in the centrality of collisions. MPI is dependent on how much the protons overlap (Section 6.4). Contribution of FSR and ISR is small therefore the most particles comes from MPI. Because of the obvious pedestal it seems that collisions start to be central at around 5 GeV.
Both Pythia8 tune differs from the data maximally by 13 % at lower p_T^{lead}. The situation is a bit worse for Herwig. At first Herwig overshoots the data by 20 % following by steep fall and undershooting of the data also by around 20 %. As the momentum of the leading track rises, all MCs start to describe the data better. It seems that Monash and Herwig fit the data in the transverse region very well from 6 GeV and higher and their description is not bad even for toward and away region. Description of A2 is on the other hand slightly better for toward and away regions than for transverse region.

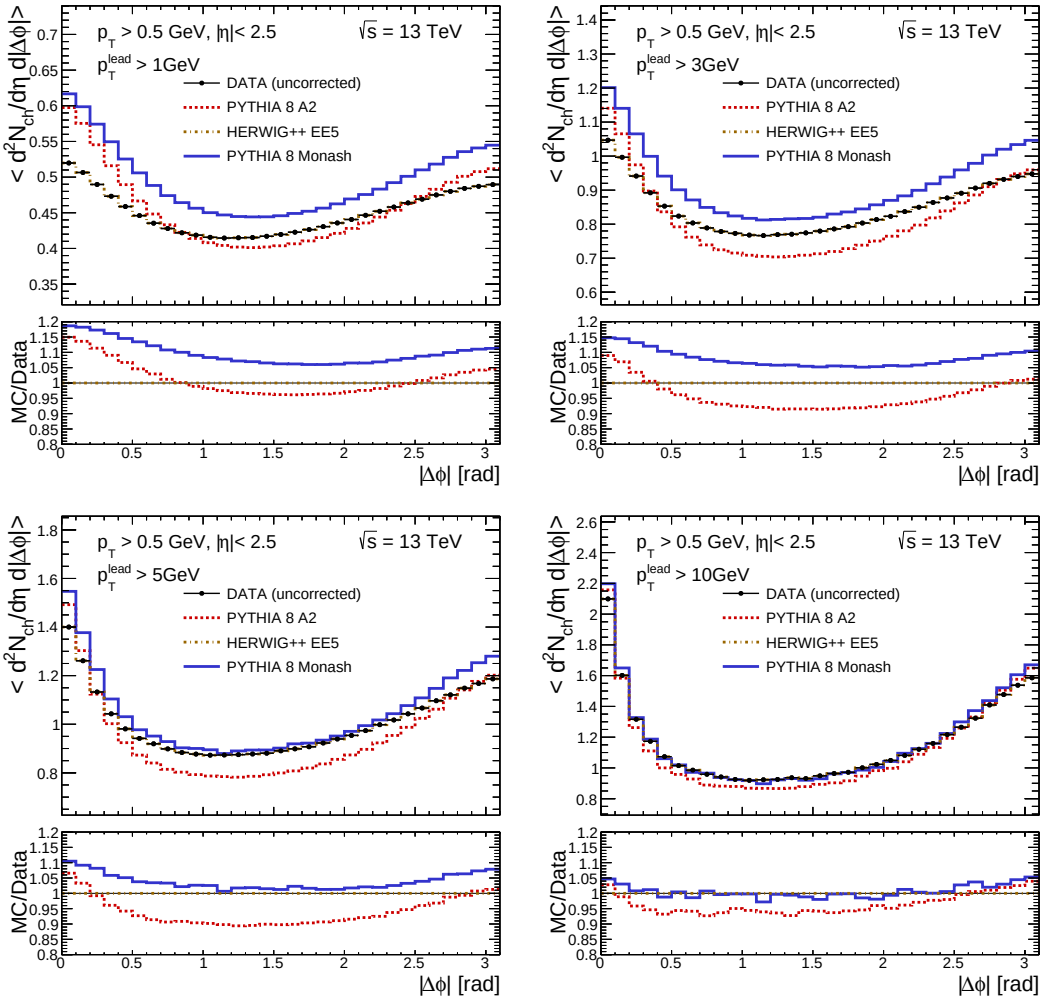

Fig. 8.3: Mean number of tracks per unit η-ϕ vs $|\Delta\phi|$ for p_T^{lead} > 1,3,5 and 10 GeV, leading track excluded.

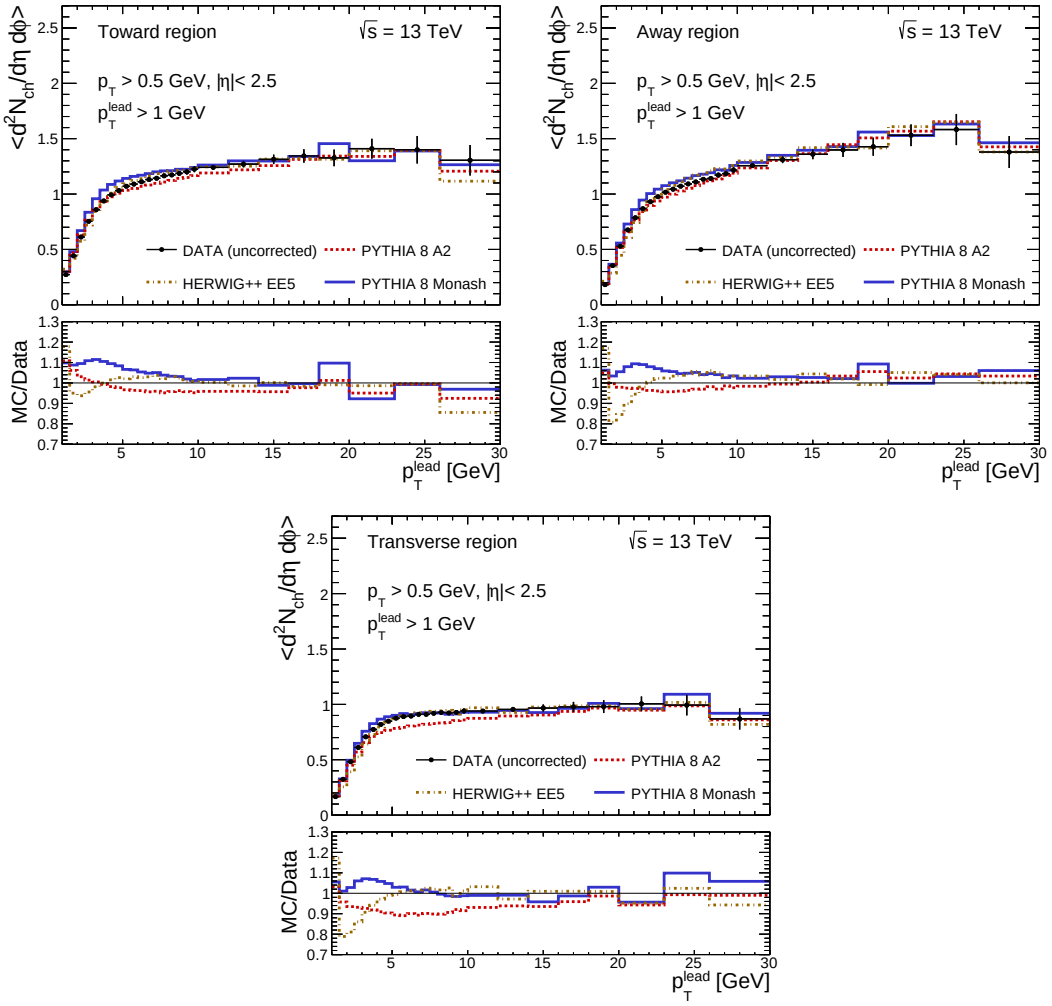

Fig. 8.4: Mean number of tracks per unit η-ϕ as a function of p_T^{lead} in toward, away and transverse region.

8.2.2 Scalar sum p_T

Σp_T **vs** $|\Delta\phi|$

The shape of mean scalar p_T sum of tracks with respect to $|\Delta\phi|$ in Fig. 8.5 resembles the multiplicity distribution in Fig. 8.3. Normalization of the distribution is done in the same way as for multiplicity versus $|\Delta\phi|$. As with the particle density the relation between Monash and the data for scalar sum p_T is improving with the rise of p_T^{lead} cut. The same applies for Herwig++ and the data whereas A2 shows the opposite effect because it is the MB tune.

Σp_T **vs** p_T^{lead}

In Fig. 8.6 mean scalar p_T sum of tracks in the toward, away and transverse region is shown against p_T^{lead}. The steep rise can be seen for all regions from 1 GeV to 5 GeV. The toward region contains the leading track therefore has obviously the highest activity, compared to other regions, which is from 5 GeV steadily rising with p_T^{lead}. The away region also rises with higher p_T^{lead} but not as much as in the toward. On the other hand in the transverse region, mean scalar p_T sum of tracks has a slow rise only by 20 % between 5 - 30 GeV.
The difference between the MCs and the Data is the highest again in the lower values of p_T^{lead}. The A2 describes very well the toward region from 5 GeV and the difference in lower p_T^{lead} is within 5 %. Good comparison between the Data and Monash in toward region starts at around 10 GeV. Similar behaviour for Monash as in the toward is also in the away but A2 slightly changes. Whereas A2 describes both previous region quite well the transverse is not in such a good agreement. The difference within the whole p_T^{lead} range is on average 10 % with the highest value of 15 % at around 7 GeV. Herwig shows similar quick change of deviation from the data at low p_T^{lead} as for N_{ch} distribution. The rest of the spectra for all region is then described reasonably well. Monash and Herwig results are better than A2 but not as good as in the transverse for particle density where from $p_T^{lead} > 7$ GeV they fit almost perfectly.

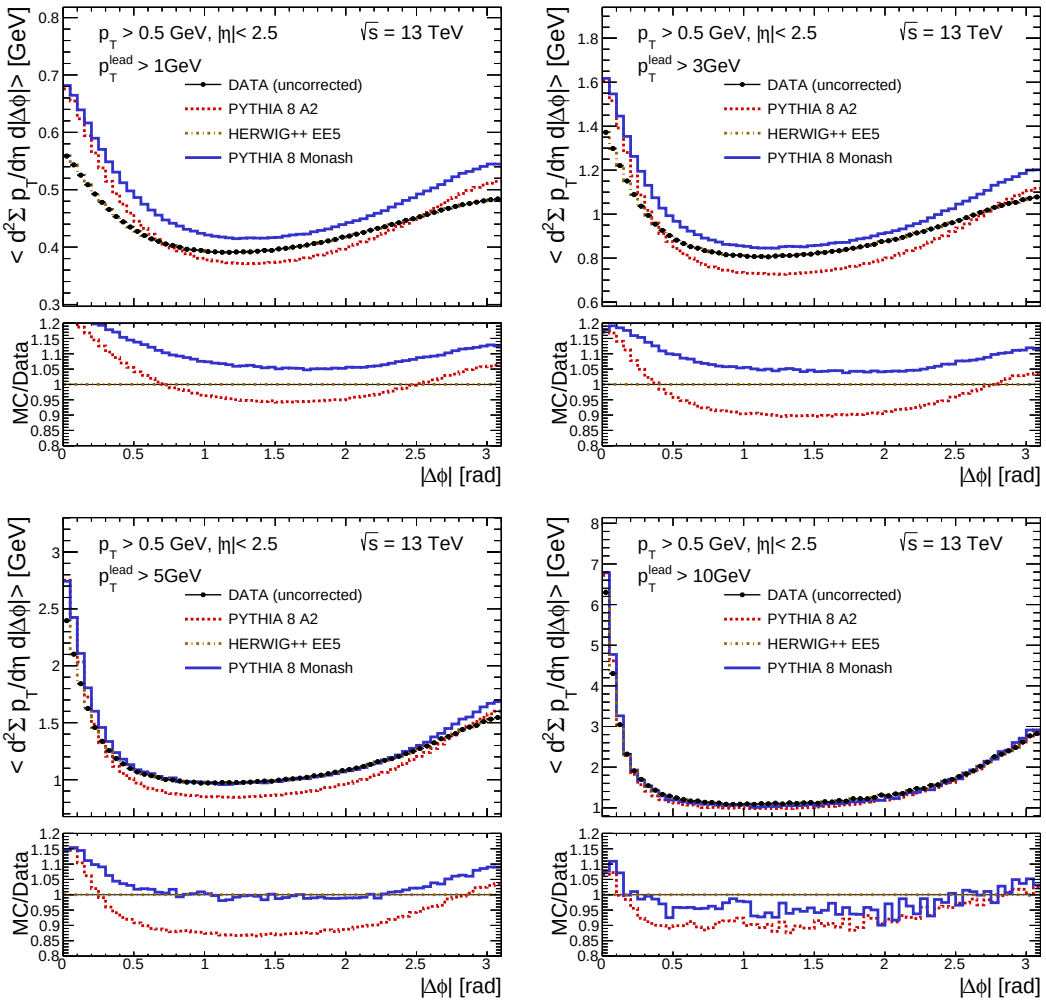

Fig. 8.5: Mean scalar p_T sum of track per unit η-ϕ with respect to $\Delta\phi$ for $p_T^{lead} >$ 1,3,5 and 10 GeV, leading track excluded.

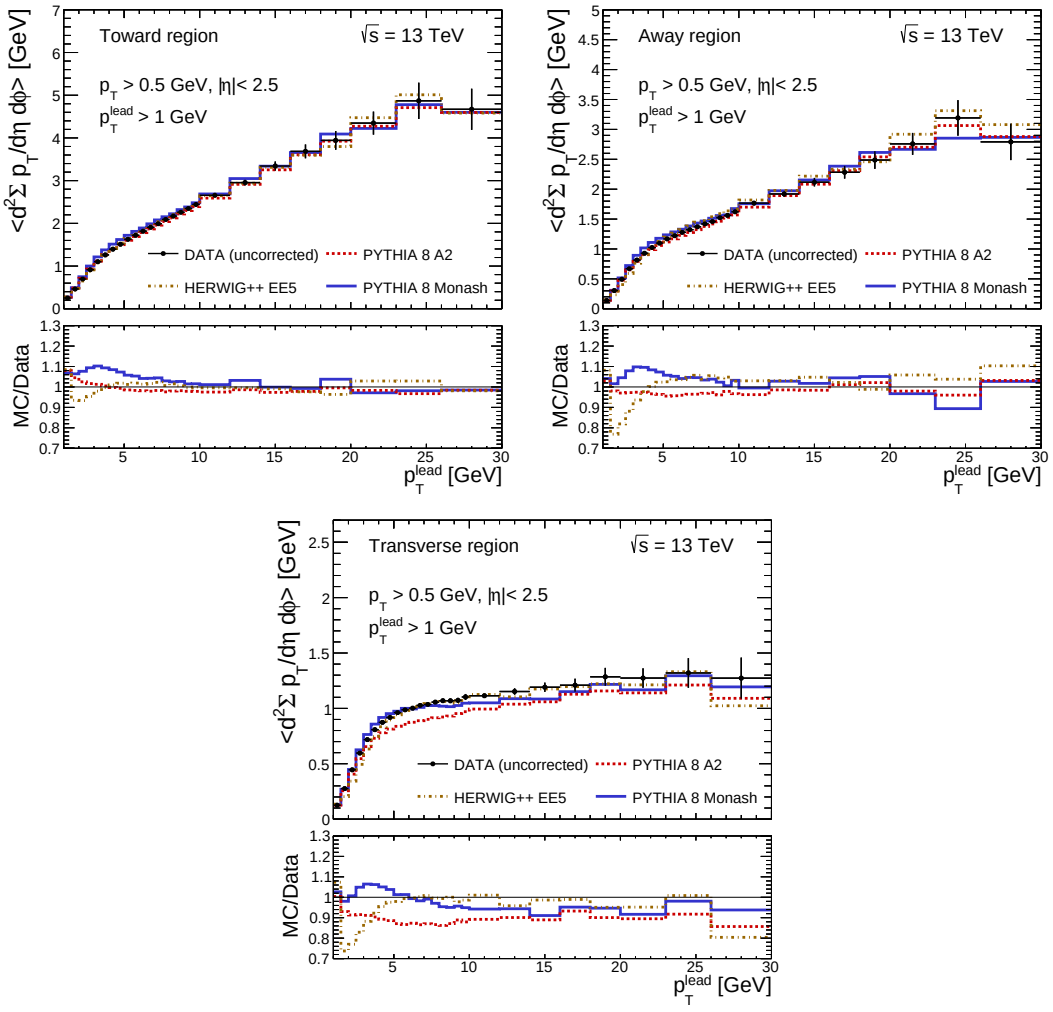

Fig. 8.6: Mean scalar p_T sum of track per unit η-ϕ with respect to p_T^{lead} in the toward, away and transverse regions.

8.2.3 Mean p_T

$< p_T >$ **vs** p_T^{lead}

The behaviour of mean p_T with respect to the p_T^{lead} is depicted in Fig. 8.7. The results can be to a certain point expected from previous figures. The rise of mean p_T can be observed for toward and away regions within the whole range whereas the transverse keeps almost the plateau from 5 GeV. The reason for higher mean p_T with rising p_T^{lead} lies in colour reconnection. Less particles are produced in hadronization process due to the reconnection of colour charge.
All MCs describe reasonably well the toward region. The picture breaks for Pythia8 family at higher p_T^{lead} in both away and transverse region. Herwig, on the other hand, seems to be able to describe all three regions.

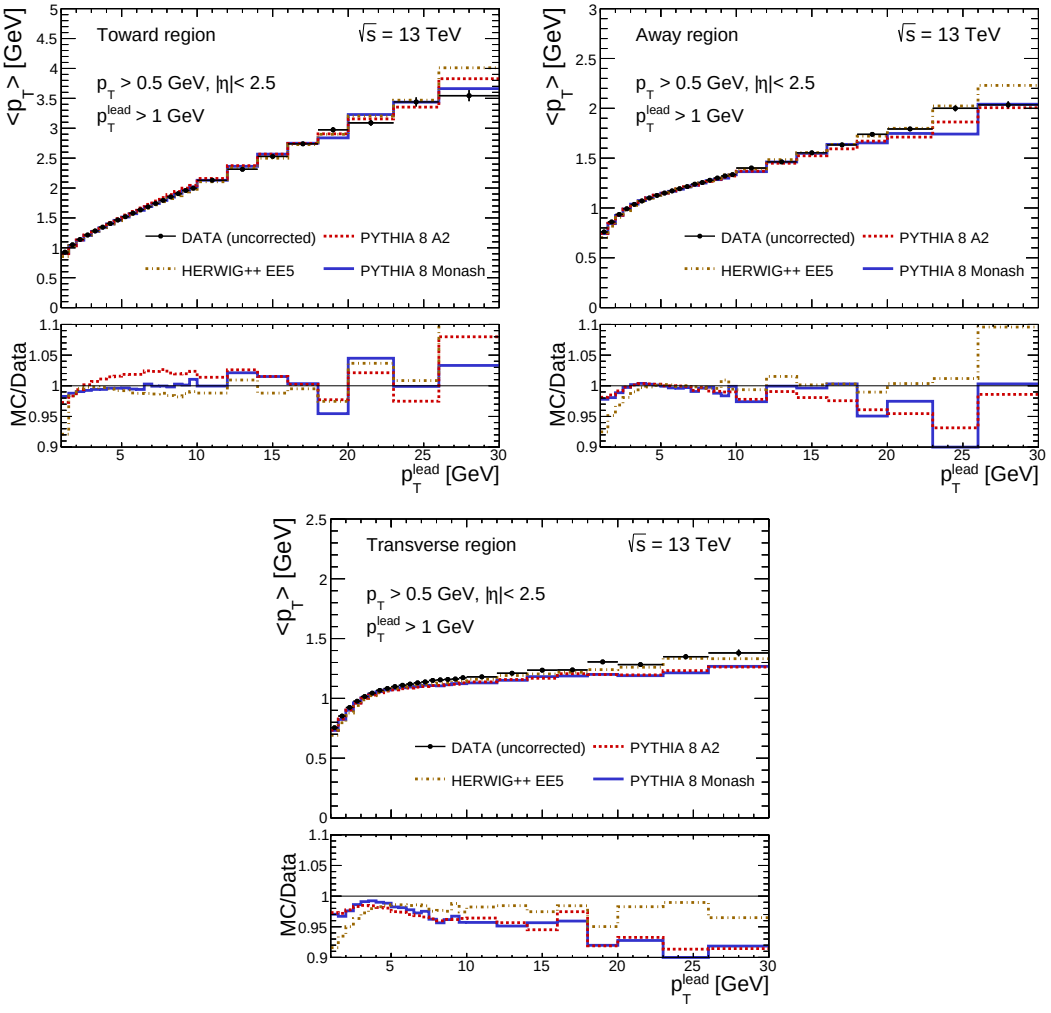

Fig. 8.7: Mean p_T of tracks with respect to the p_T^{lead} in the toward, away and transverse regions.

$< p_T >$ vs $\mathbf{N}_{ch}$

The mean p_T with the respect to the number of tracks in the certain region is depicted in Fig. 8.8. The decrease of mean p_T in the toward region at low N_{ch} is because the leading track has major contribution to the p_T in comparison with other tracks. Therefore, when additional track is added the mean p_T drops down. At around 6 GeV mean p_T starts to rise. The behaviour in the transverse and away is almost similar and the rise of 20% through the whole range can be seen.
The difference between the MCs and the data is within 5 % at lower N_{ch} for all MCs. Monash seems to be best for description of the data at higher N_{ch} whereas A2 is better for low N_{ch}.

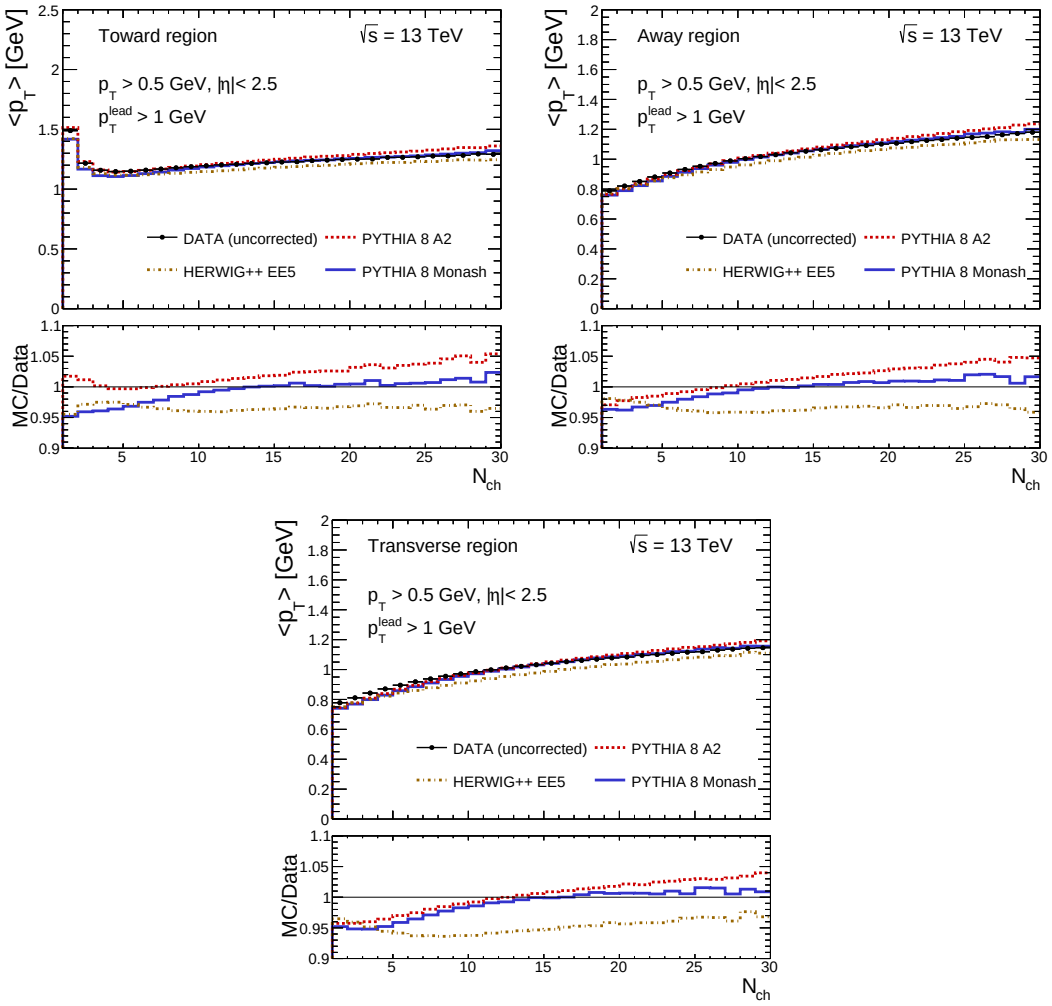

Fig. 8.8: Mean p_T of tracks with respect to the number of charged particles N_{ch} in selected regions.

8.3 Corrections

As was mentioned earlier correction are used to obtain particle level and are determined from MC. The next step would be to apply correction to all plots presented in results. The correction procedure to the UE event measurement has started, but unfortunately has not been completed yet. Nevertheless, some of the first systematic corrections were done and can be seen in Section 8.4. However, first application of correction has to be presented.

It can occur that tracks from event are not reconstructed which leads to loss of tracks. A following weight had to be applied to all track-level histograms.

$$w_{trk} = \frac{1}{\epsilon_{bin}(p_T, \eta)} \cdot (1 - f_{okr}(p_T, \eta) - f_{sec}(p_T, \eta) - f_{strangebar}(p_T)) \tag{8.1}$$

The first term $\epsilon_{bin}(p_T, \eta)$ is the track-reconstruction efficiency, f_{okr} is a fraction of tracks out of kinematic region (e.g from $|\eta| > 2.5$) which migrates to the "visible" region, f_{sec} represent fraction of secondary particles (particles which don't fit the definition of primary), and $f_{strangebar}$ fraction of strange baryons. Prediction rate of strange baryons is strongly model dependent, while there is negligible efficiency to reconstruct them at detector level due to the kink in the detector which these particles create (e.g $\Sigma^+ \to pn$). Consequently they are either not seen at all, or the momentum is badly reconstructed as some energy is carried away by the neutral daughter particle.

$$\epsilon_{bin}(p_T, \eta) = \frac{N_{rec}^{matched}(p_T, \eta)}{N_{gen}(p_T, \eta)} \tag{8.2}$$

$N_{rec}^{matched}(p_T, \eta)$ is the number of reconstructed tracks in a given bin matched to a generated particle and $N_{gen}(p_T, \eta)$ is the number of generated particles in the same bin.

In order to account for events which were not reconstructed (leading track might not be reconstructed leading to failing criterions and rejection of the event) event correction needs to be applied also through weight.

$$w_{evt} = \frac{1}{\epsilon_{trig}(N_{sel}^{BS})} \frac{1}{\epsilon_{vtx}(N_{sel}^{BS})} \frac{1}{\epsilon_{leadtrk}(\epsilon_{trk})} \tag{8.3}$$

The first term is to account for trigger efficiency in particular for MBTS. The next is efficiency of vertex reconstruction and the last term is to correct for failing the event precisely due to the case with leading track given above. As mentioned before condition $p_T^{lead} > 1$ GeV causes that $w_{evt} \approx 1/\epsilon_{leadtrk}(\epsilon_{trk})$

8.4 Additional results (EPS plots)

New set of plots for EPS (European physical society) conference, as addition to UE analysis and thesis assignement, was made and can be seen in Fig. 8.9 and Fig. 8.10. Convenors of Standard Model asked these plots to be prepared with systematic uncertainty. This uncertainty represents bad material modeling of detector meaning that the detector has more material than expected. If the detector has more material obviously more tracks can be lost. Therefore, this effect has to be accounted for. The value of uncertainty was determined by randomly removing tracks (after selection) according to tracking efficiency uncertainty (Section 8.3). The errors were symetrized.
In addition to Herwig, A2 and Monash two more MCs are being compared with the data. The first one is another from Pythia8 family A14 [27] in which tunning of MPI, ISR, FSR free parameters has been performed in a single step with help of UE data from Run I. The second one is Epos [30] which includes QCD-inspired field theory that desribes the hard and soft scattering simultaneously. This brings advantage for calculation which no longer depends on PDFs.

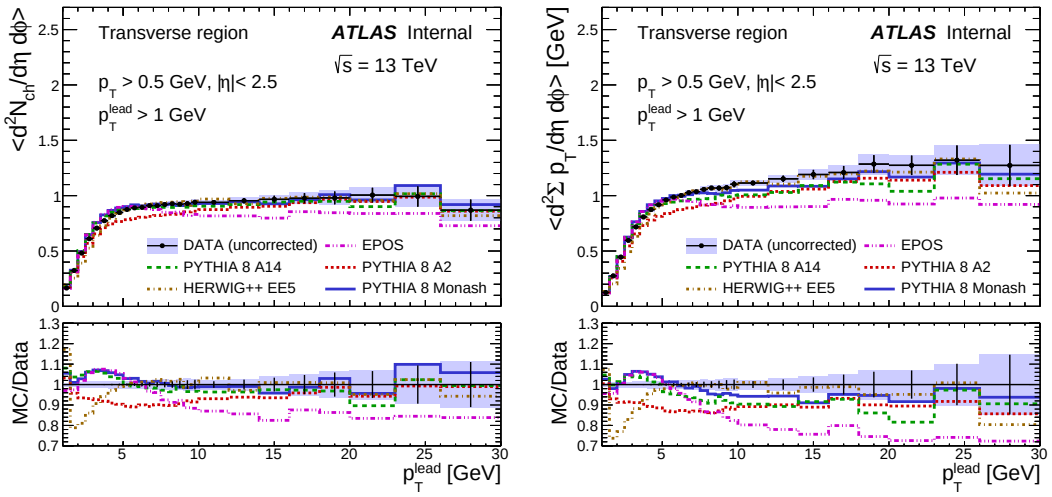

Fig. 8.9: Mean number of selected tracks per unit $\eta - \phi$ vs p_T^{lead} on the left and mean scalar p_T sum of selected tracks per unit $\eta - \phi$ vs p_T^{lead} on the right. Both distributions are in transverse region. The data are compared with MC on detector level. The shaded bands represent the combined statistical and systematic uncertainties, while the error bars show the statistical uncertainties.

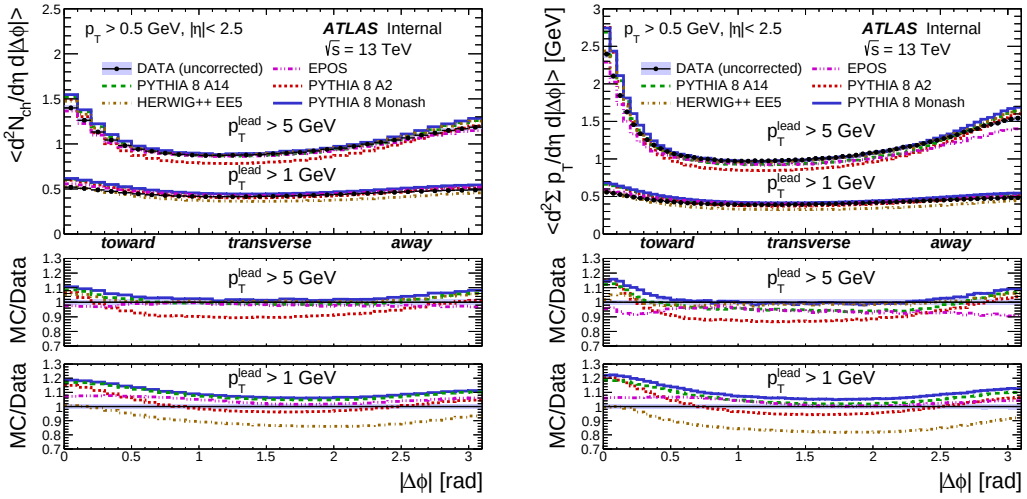

Fig. 8.10: Mean number of selected tracks per unit $\eta-\phi$ vs $|\Delta\phi|$ on the left and mean scalar p_T sum of selected tracks per unit $\eta-\phi$ vs $|\Delta\phi|$ on the right. Top pad contains distribution for $p_T^{lead} > 1$ GeV and $p_T^{lead} > 5$ GeV. Middle and bottom pad represent ratio for $p_T^{lead} > 5$ GeV and $p_T^{lead} > 1$ GeV respectively. The data are compared with MC on detector level. The shaded bands represent the combined statistical and systematic uncertainties, while the error bars show the statistical uncertainties.

Chapter 9

Summary

The process of pp collision is a complicated topic and this thesis tried to summarize and explain its fundamental parts important for particle creation. However, the main purpose of this project was to analyse the UE at 13 TeV measured with ATLAS and compare data from Run II with several MC models as soon as possible.

For fullfilling the task, it was necessary to obtain some programming knowledge in C++ and in ROOT as it was decided that the code would be based on SFRAME (C++ package).

The comparison between data and MCs was done basically two weeks after the receipt of data and were provided in Section 8.2. The objects of study were mean scalar p_T sum of tracks $< \mathrm{d}^2\Sigma p_T / \mathrm{d}\eta\,\mathrm{d}\phi >$ per unit $\eta - \phi$, mean number of charged particles $< \mathrm{d}^2 N_{ch} / \mathrm{d}\eta\,\mathrm{d}\phi >$ per unit $\eta - \phi$ and the mean transverse momentum $< p_T >$.

Neither one of the presented MC (Pythia8 Monash, Pythia8 A2, HERWIG++) does describe well all the observables. However, it could be said that all MCs are tuned reasonably well and there are no significant difference compared to data. Therefore, MCs don't have to be retuned which is surely good news. As was mentioned, Monash and Herwig++ are UE tunes and thus describe best the transverse region (most sensitive region to the UE). The comparison is even better for higher p_T^{lead} where jets can arrise. A2 as MB tune is better at describing lower p_T^{lead} and the toward and away region.
The difference between particle activity at 7 TeV [4] and at 13 TeV is roughly around 20%.
After writing the UE analysis code, in awaiting for data, closure tests of Monash (only available at the time) on detector and particle level was studied for correction on particle level which is the next step for this thesis.
Because the results of UE study at 13 TeV were done quite fast after data collection and also because they can contain usefull information to some measurements, they are going to be presented at European physical society (EPS) on high energy physics (HEP) which is held in Vienna between 22-29th july 2015 [34].

Bibliography

[1] The CDF collaboration, *The underlying event in hard interactions at the Tevatron $\bar{p}p$ collider*, Phys. Rev. D70 (2004), FERMILAB-PUB-04-041-E

[2] The CDF collaboration *Studying the underlying event in Drell-Yan and high transverse momentum jet production at the Tevatron*, Phys. Rev. D82 (2010)

[3] The CMS collaboration, *First Measurement of the Underlying Event Activity at the LHC with $\sqrt{s} = 0.9$ TeV*, Eur.Phys.J. C70 (2010), CERN-PH-EP-2010-014

[4] The ATLAS collaboration, *Measurement of underlying event characteristics using charged particles in pp collisions at $\sqrt{s} = 900$ GeV and 7 TeV with the ATLAS detector*, Phys. Rev. D83 (2011), CERN-PH-EP-2010-063

[5] Wikipedia, *The Standard Model of Elementary Particles*, cited 23.6. 2015 `http://commons.wikimedia.org/wiki/File:Standard_Model_of_Elementary_Particles.svg`,

[6] W. Rindler, *Relativity, Special, General and Cosmological*, Oxford University Press Inc. (2006)

[7] M. Riordan, *The Discovery of Quarks*, (1992), SLAC-PUB-5724

[8] Richard D. Ball, Valerio Bertone, Stefano Carrazza, Christopher S. Deans, Luigi Del Debbio, Stefano Forte, Patrick Groth Merrild , Alberto Guffanti, Nathan P. Hartland, Zahari Kassabov, José I. Latorre, Juan Rojo, Luca Rottoli, Maria Ubiali, *Neural Network Parton Distribution Functions*, `https://nnpdf.hepforge.org/`

[9] Wu Ki-Tung (Scholarpedia), *Bjorken scalling*, Oxford University Press Inc., `http://www.scholarpedia.org/article/Bjorken_scaling`

[10] H. Jung, *Multiparton interaction and underlying events at HERA and the LHC*, (2009), `http://www.desy.de/~jung/talks/multiple-interactions.pdf`

[11] Sjostrand, Torbjorn, *Monte Carlo Tools*, (2009), LU-TP-09-31, MCNET-09-17

[12] Seymour, Michael H. and Marx, Marilyn, *Monte Carlo Event Generators*, (2013), "MCNET-13-05

[13] Bahr, Manuel and Butterworth, Jonathan M. and Seymour, Michael H., *The Underlying Event and the Total Cross Section from Tevatron to the LHC*, (2009), CERN-PH-TH-2008-129, KA-TP-13-2008 MCNET-08-03",

[14] Corke, Richard and Sjostrand, Torbjorn, *Interactions and Rescattering*, (2010), LU-TP-09-28, MCNET-09-16

[15] Corke, Richard and Sjostrand, Torbjorn, *Multiparton Interactions with an x-dependent Proton Size*, (2011), LU-TP-11-06, MCNET-11-03

[16] Joao Pequenao, *Computer generated image of the whole ATLAS detector*, (2008), CERN-GE-0803012, `http://cds.cern.ch/record/1095924`

[17] Joao Pequenao and Paul Schaffner, *An computer generated image representing how ATLAS detects particles*, (2013), CERN-EX-1301009 , `https://cds.cern.ch/record/1505342`

[18] Kanai, Tsubasa and Jinnouchi, Osamu, *Measurement of the material in the ATLAS Inner Detector using hadronic interactions for an improvement in the track reconstruction*, (2013), CERN-THESIS-2013-017, `https://cds.cern.ch/record/1528163`

[19] Höche, Stefan, *Introduction to parton-shower event generators*, (2014), SLAC-PUB-16160

[20] ATLAS collaboration", *Charged-particle multiplicities in pp interactions measured with the ATLAS detector at the LHC*, (2011), CERN-PH-EP-2010-079

[21] Buckley, Andy and Butterworth, Jonathan and Gieseke, Stefan and Grellscheid, David and Hoche, Stefan and others, *General-purpose event generators for LHC physics*, (2011), CAVENDISH-HEP-10-21

[22] B. Povh, K. Rith, Ch. Scholz, F. Zeutsche, *Particles and Nuclei, An introduction to the Physical Concepts*, (1999)

[23] J. C. Collins, *Sudakov Form Factor*, (2003), arXiv:hep-ph/0312336

[24] T. Sjöstrand, M. van Zijl *A Multiple Interaction Model for the Event Structure in Hadron Collisions*, Phys.Rev. D36 (1987), `http://home.thep.lu.se/~torbjorn/preprints/lutp8705.pdf`

[25] F Hügging, *The ATLAS Pixel Insertable B-Layer (IBL)*, (2010), arXiv:1012.2742v1

[26] ATLAS Collaboration, *Further ATLAS tunes of PYTHIA6 and Pythia 8*,(2011), ATL-PHYS-PUB-2011-014, `https://cds.cern.ch/record/1400677` .

[27] ATLAS Collaboration, *ATLAS Run 1 Pythia8 tunes*, (2014), ATL-PHYS-PUB-2014-021, `https://cds.cern.ch/record/1966419`

[28] S. Gieseke, C. Rohr, and A. Siodmok, *Colour reconnections in Herwig++*, Eur. Phys. J. C72 (2012) 2225, arXiv:1206.0041

[29] P. Skands, S. Carrazza, and J. Rojo, *Tuning PYTHIA 8.1: the Monash 2013 Tune*, Eur. Phys. J. C74 (2014) 3024, arXiv:1404.5630

[30] T. Pierog, I. Karpenko, J. Katzy, E. Yatsenko, and K. Werner, *EPOS LHC : test of collective hadronization with LHC data*, arXiv:1306.0121

[31] Cian O'Luanaigh *LHC: Preparations for collisions at 13 TeV* `http://home.web.cern.ch/about/updates/2015/04/lhc-preparations-collisions-13-tev`

[32] Special thanks to Jan Lochman for providing pictures from his presentation *Hight p_T jets in Run II of the ATLAS Experiment*

[33] E. Nurse, T. Kuhl, and A. K. Morley, *Draft for 13 TeV minimum bias paper*, (2015), ATL-COM-PHYS-2015-346, `https://cds.cern.ch/record/2013322`

[34] Oldřich Kepka, Deepak Kar, Matouš Vozák, *Leading Track Underlying Event at 13 TeV*, (2015), ATL-COM-PHYS-2015-602, `https://cds.cern.ch/record/2030164`